Solar photoelectro-Fenton-like process with anodically-generated HClO in a flow reactor: Norfloxacin as a pollutant with a particular structure

María F. Murrieta [a,b], Enric Brillas [b], José L. Nava **,[a], Ignasi Sirés *,[b]

[a] *Departamento de Ingeniería Geomática e Hidráulica, Universidad de Guanajuato, Av. Juárez 77,*

Zona Centro, C.P 36000, Guanajuato, Guanajuato, Mexico

[b] *Laboratori d'Electroquímica dels Materials i del Medi Ambient, Departament de Ciència de*

Materials i Química Física, Secció de Química Física, Facultat de Química, Universitat de

Barcelona, Martí i Franquès 1-11, 08028 Barcelona, Spain

Paper submitted to be published in the

Journal of Environmental Chemical Engineering

*Corresponding author: i.sires@ub.edu (I. Sirés)

** Corresponding author: jlnm@ugto.mx (J.L. Nava)

Abstract

The degradation and mineralization of the drug norfloxacin (NFX) has been assessed in a model solution, containing 15 mM NaCl + 45 mM Na_2SO_4 at pH 3.0, using a flow plant with an FM01-LC filter-press reactor equipped with a Ti|Ir-Sn-Ru oxides anode to electrogenerate HClO from Cl^- oxidation and a stainless-steel cathode. Unexpectedly, anodic oxidation with active chlorine (AO-HClO) outperformed electro-Fenton (EF-HClO), photoelectro-Fenton (PEF-HClO) and solar photoelectro-Fenton (SPEF-HClO) due to: (i) the formation of refractory complexes between iron ions and carboxyl group of NFX, and (ii) the conversion of HClO into less effective $^\bullet$OH upon its Fenton-like reaction with added Fe^{2+} catalyst. SPEF-HClO was superior among Fenton-based treatments because the $^\bullet$OH concentration was largely increased by the photolysis of Fe(III) species. At an initial NFX concentration in the range 0.103-0.146 mM, the optimum conditions for SPEF-HClO were 0.40 mM Fe^{2+} and 15 mA cm^{-2}. A BDD anode allowed a higher production of $^\bullet$OH, accelerating the degradation and mineralization, with similar energy requirements as compared to trials with Ti|Ir-Sn-Ru oxides anode. The SPEF-HClO process in urban wastewater was less powerful because of the parallel oxidation of natural organic matter. HClO, Fe^{2+} and Fe_{total} were quantified in both water matrices. The initial degradation sequence for NFX, proposed from 10 primary by-products identified by LC-MS/MS, revealed the occurrence of hydroxylation, chlorination and defluorination steps. Additionally, 5 stable by-products were detected by GC-MS.

Keywords: Anodic oxidation; Electro-Fenton; Pharmaceutical residue; Solar photoelectro-Fenton; Urban wastewater; Water treatment

1. Introduction

As a result of the major importance acquired by the treatment of diseases in animals and humans, the consumption of antibiotics has grown exponentially worldwide, especially in high-income countries [1]. Due to their chemical properties and persistence, antibiotics have been detected in many water bodies like wastewater treatment plants, hospital effluents and surface water [2,3]. The accumulation of drug residues in natural water resources has become a threat because of their potential or confirmed adverse effects on living beings. To mitigate this problem, it is important to develop efficient wastewater treatment technologies against antibiotics.

In this context, advanced oxidation processes (AOPs) appear as a viable technology to eliminate these contaminants thanks to the in-situ production of strong oxidants, mainly the hydroxyl radical ($^{\bullet}$OH). Several AOPs like UV/H_2O_2, photocatalysis, Fenton-based processes, chlorination and ozonation have shown their ability to eliminate antibiotics from aqueous media [4]. More specifically, the electrochemical advanced oxidation processes (EAOPs) have emerged to overcome several drawbacks of the AOPs, such as high consumption of energy or reagents in some cases [5]. In EAOPs, the generation of $^{\bullet}$OH can occur at the anode surface from water oxidation, as shown in reaction (1) which is pre-eminent in the anodic oxidation process (AO). Owing to its capability to yield very active physisorbed $^{\bullet}$OH, the best performance in AO in terms of oxidation of organic pollutants has been reached using the boron-doped diamond anode (BDD) [6].
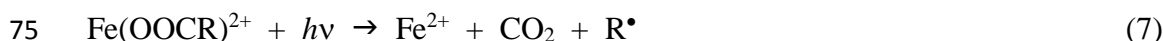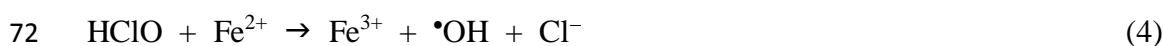
$$M + H_2O \rightarrow M(^{\bullet}OH) + H^+ + e^- \tag{1}$$

Furthermore, EAOPs can yield homogeneous $^{\bullet}$OH in the bulk through chemical reactions favored by electrogenerated species. For example, H_2O_2 can be electrogenerated on carbonaceous cathodes to induce the Fenton's reaction in the so-called electro-Fenton (EF) process, which has been widely evaluated in the elimination of antibiotics [7-9]. Since wastewater usually contains chloride ions, active chlorine can be produced anodically, thereby affecting the EF process [10]. In a chloride

medium, the generation of active chlorine species occurs by the oxidation of the anion via reaction (2) to produce dissolved chlorine ($E° = 1.36$ V/SHE) at pH up to 3. Cl_2 is converted into HClO ($E° = 1.49$ V/SHE) according to reaction (3) within the pH range 3-8. At pH >8, deprotonation is favored, yielding ClO^- ($E° = 0.89$ V/SHE) [11]. Several works have shown the ability of anodic oxidation mediated by active chlorine species (AO-HClO) for the elimination of organic pollutants, including pharmaceuticals [12,13].

$$2Cl^- \rightarrow Cl_2(aq) + 2e^- \qquad (2)$$

$$Cl_2(aq) + H_2O \rightarrow HClO + Cl^- + H^+ \qquad (3)$$

Nonetheless, in the presence of Fe(II), the active chlorine species can be transformed into $^\bullet OH$ via Fenton-like reaction (4), giving rise to an electro-Fenton-like (EF-HClO) process with great effectiveness to degrade organic compounds [14,15]. The Fe(II) catalyst can be continuously regenerated by the reduction of the Fe(III) at the cathode surface via reaction (5). Otherwise, the irradiation of the solution with UVA light can also enhance the Fe(II) regeneration from photolytic reactions (6) and (7) in the so-called photoelectro-Fenton-like and solar photoelectro-Fenton-like (PEF-HClO and SPEF-HClO), propagating the $^\bullet OH$ production via reaction (4) [16-21].

$$HClO + Fe^{2+} \rightarrow Fe^{3+} + {}^\bullet OH + Cl^- \qquad (4)$$

$$Fe^{3+} + e^- \rightarrow Fe^{2+} \qquad (5)$$

$$Fe^{3+} + h\nu \rightarrow Fe^{2+} + {}^\bullet OH \qquad (6)$$

$$Fe(OOCR)^{2+} + h\nu \rightarrow Fe^{2+} + CO_2 + R^\bullet \qquad (7)$$

In previous works, the PEF-HClO and SPEF-HClO processes were applied to the elimination of the azo dyes Acid Red 1 and Acid Yellow 36 [22,23], the antibiotic sulfamethoxazole [24] and the herbicide picloram [25]. In all cases, the viability of the Fenton-like process was demonstrated. However, the influence of the chemical structure of the target molecule on the process is still unclear. A previous work performed by Gozzi et al. [26] evaluated the mineralization of the herbicide

tebuthiuron (TBH) by EF in sulfate medium, obtaining different kinetic rates, which was attributed

to the formation of recalcitrant Fe(III)-TBH complexes. Furthermore, the influence of the structure

on the removal of four triphenylmethane dyes by EF was evaluated in a research performed by Sirés

et al. [27]. In that study, a different removal rate was observed for each dye, being attributed to the

presence of different types of substituents that conferred recalcitrance to the pollutants.

In the present work, norfloxacin (NFX) has been selected as a model contaminant, in order to

assess the potential impact of the structure (i.e., presence of a carboxyl group) on the performance of

HClO-mediated electrochemical Fenton-based process. NFX is a fluoroquinolone widely used for the

treatment of respiratory infections, urinary tract infections and infections caused by bacteria like

Escherichia coli [28,29]. In addition, the NFX is ranked within the most common quinolones detected

in wastewater and natural water resources, attaining concentrations of ng L^{-1} to µg L^{-1} [30,31]. Some

authors reported that NFX can induce DNA damage, cytotoxic and genotoxic effects in aquatic

organisms, also stimulating the antibiotic resistance of bacteria [32,33]. The removal of NFX has

been evaluated by UV/H_2O_2 [31,34], photocatalysis [35-37], Fenton-based processes [38,39] and

photocatalysis with active chlorine species [40,41], as well as by other methods [42,43]. The

elimination of NFX has also been carried out by AO with BDD anode [44-46], AO-HClO [47,48],

homogeneous EF [49] and heterogeneous EF [50]. It is important to mention that, as far as we are

concerned, the elimination of NFX by Fenton-like processes using electrogenerated HClO has not

been evaluated so far.

In this work, the trials were carried out in a 3-L pre-pilot plant equipped with an FM01-LC filter-

press flow cell, which included a Ti|Ir-Sn-Ru oxides anode and a stainless-steel cathode, coupled to

a photoreactor operating in recirculation batch mode. A mixed supporting electrolyte, containing 15

mM NaCl + 45 mM Na_2SO_4, and urban wastewater were employed as matrices. Note that the former

is a synthetic medium that has been previously optimized to have a chloride content and specific

conductivity similar to those of the actual wastewater matrix [24]. The influence of the Fe(II)

concentration, current density (j) and initial NFX concentration was addressed. The NFX content was taken much higher than that found in actual wastewater to ease the determination of the degradation and mineralization percentages, as well as the detection of intermediates and final products. The performance of AO-HClO, EF-HClO, PEF-HClO and SPEF-HClO trials was compared to elucidate the role of the molecule structure on the degradation performance. Some comparative SPEF-HClO assays were made with the powerful BDD anode, aiming to demonstrate that a cheaper Ti|Ir-Sn-Ru oxides anode can be adopted to destroy NFX. The generated carboxylic acids were identified by ion-exclusion high-performance liquid chromatography (HPLC), whereas the main degradation by-products were detected by gas chromatography-mass spectrometry (GC-MS) and liquid chromatography-mass spectrometry (LC-MS/MS), aiming at proposing a degradation route for the treatment of NFX.

2. Materials and methods

2.1. Chemicals

NFX ($\geq$ 98% purity) was purchased from Sigma-Aldrich and used as received. Analytical grade NaCl (Panreac) and Na_2SO_4 (Merck) served to prepare the synthetic solutions. $FeSO_4 \bullet 7H_2O$ (analytical grade, Merck) was added as catalyst in Fenton-based processes. Solution pH was always adjusted to 3.0 with analytical grade H_2SO_4 (Merck) because this value is needed to keep the iron catalyst soluble [5]. Other chemicals required to carry out the analyses were provided by Sigma-Aldrich, Panreac, Merck and Fluka. Synthetic solutions were prepared with deionized water and analytical solutions with high-purity water from a Millipore Milli-Q system (resistivity > 18.2 MΩ cm at 25 °C).

2.2. Aqueous matrices

Two types of solutions were used in the present work. The oxidation ability of the SPEF-HClO process was tested with a synthetic solution containing 15 mM NaCl + 45 mM Na_2SO_4. (i.e., Cl^-

content similar to that of urban wastewater, high enough to electrogenerate sufficient HClO under the chosen electrolytic conditions). The study was further extended to a wastewater treatment plant (WWTP) effluent (i.e., secondary treatment), collected from a municipal plant located in Gavà (Spain) and maintained in a refrigerator at 4 ºC before use. This complex matrix contained organic pollutants, including natural organic matter (NOM) like fulvic and humic acids, and had the following characteristics: pH 7.7, electrical conductivity of 2.6 mS cm^{-1}, 11.0 mg L^{-1} TOC; its ion composition (in mg L^{-1}) was: Na$^+$ (145.0), K$^+$ (41.8), Ca^{2+} (114.3), Mg^{2+} (31.6), Fe^{2+}/Fe^{3+} (0.18), SO$_4^{2-}$ (146.2), Cl$^-$ (361.1) and NO$_3^-$ (< 1).

2.3. Flow plant

Fig. 1 shows a scheme of the experimental setup of the solar flow plant constructed in our laboratory for the present work. The electrochemical cell was a commercial FM01-LC filter-press reactor equipped with a Ti|Ir-Sn-Ru oxides anode plate and a stainless-steel plate as the cathode, both with a geometric area of 64 cm^2 and separated by a gap of 0.55 cm. To improve the mass transport, a type-D turbulence promoter was placed between the anode and cathode. The anode was synthesized as previously described [24], using Ru as doping agent to improve the anodic transformation of chloride into chlorine. In some assays, a Nb|BDD thin film of the same area (NeoCoat) was used as the anode.

In all the assays, 3 L of solution was introduced in a reservoir (capacity > 3 L) and consecutively recirculated through the electrochemical reactor and a solar planar photoreactor employing a peristaltic pump. The solution temperature was regulated at 30 ºC with two heat exchangers and the liquid flow rate (LFR) was adjusted to 180 L h^{-1} with a flowmeter. The solar photoreactor made with polypropylene had dimensions of 21 cm × 21 cm × 2.5 cm, corresponding to an irradiated volume of 600 mL. It was tilted 41º (the latitude of Barcelona), with a mirror at the bottom to better concentrate the incident sunlight photons. The SPEF-HClO trials were carried out in cloudless sunny days in 2021, achieving an average UV solar irradiance (300-400 nm) of about 28-30 W m^{-2}, as determined

7

with a Kipp&Zonen CUV 5 radiometer. The duration of the experiments was limited to 300 min to avoid a significant decay of irradiance. The photoreactor was covered with a black cloth to run the AO-HClO and EF-HClO assays. In the case of the PEF-HClO experiments, the solar photoreactor was replaced by an annular photoreactor of 600 mL with a 160-W UVA Omnilux 27E lamp placed inside. All the trials were carried out under galvanostatic conditions, with current supplied by a Grelco GVD310 power source.

Replicates of all the experiments were always made, and the average values obtained are reported in this manuscript with a confidence interval of 95%.

2.4. Instruments and analytical procedures

The solution pH and conductivity were monitored continuously during the trials. Samples collected from treated solutions were first filtered (0.45 µm PTFE syringe filters, Whatman) and then analyzed as required. Active chlorine was quantified by means of the so-called DPD colorimetric method, with measurements made at $\lambda = 515$ nm [51]. The Fe^{2+} and Fe_{total} contents were obtained from the phenanthroline method, measuring at $\lambda = 510$ nm [52]. Similarly, the NH_4^+ concentration was determined via the indophenol blue method, at $\lambda = 630$ nm [53]. For all colorimetric analyses, a Shimadzu 1800 UV/Vis spectrophotometer was used, at 25 ºC.

The NFX concentration during the treatments was evaluated by reversed-phase high-performance liquid chromatography (HPLC) using a Waters system, with the detector set at $\lambda = 278.2$ nm. The column employed for separation was a Kinetex 5 µm Biphenyl, 150 mm × 4.6 mm (i.d), thermostated at 30 °C, whereas the mobile phase was composed of 15:85 (v/v) acetonitrile/water (0.1% formic acid) and was eluted at 1.0 mL min^{-1}. In the chromatograms, the drug appeared at a retention time (t_r) of 8.9 min. The same equipment was equipped with a Bio-Rad Aminex HPX 87H, 300 mm × 7.8 mm (i.d.) column, thermostated at 35 ºC, to identify the short-chain aliphatic carboxylic acids by ion-exclusion HPLC, measuring at $\lambda = 210$ nm. A 4 mM H_2SO_4 solution was eluted as mobile phase, at 0.6 mL min^{-1}, yielding only a single peak related to formic acid at $t_r = 13.9$ min. The

evolution of F^-, Cl^- and ClO_3^- concentrations was followed by ion chromatography using a 10Avp

chromatograph from Shimadzu, coupled to a conductivity detector. Upon injection, the samples (25

μL) were eluted through a Shim-Pack IC-A1S, 100 mm $\times$ 4.6 mm (i.d.) anion column thermostated

at 40 °C, by means of a 2.6 mM phthalic acid + 2.4 mM tris(hydroxymethyl)aminomethane (pH 4)

mixture at 1.5 mL min^{-1}.

The mineralization process was quantified from the solution TOC variation, measured with an

VCSN TOC analyzer from Shimadzu. From the obtained values, the mineralization current efficiency

(MCE, in percentage) was calculated as follows:

$$\% \text{ MCE} = \frac{nFV_s\Delta(\text{TOC})_{\text{exp}}}{4.32\times10^7 mIt} \times 100 \tag{8}$$

where each term has its usual meaning [18]. The total number of electrons can be easily obtained

considering the overall conversion of all N into NH_4^+:

$$C_{16}H_{18}FN_3O_3 + 29\ H_2O \rightarrow 16CO_2 + 3NH_4^+ + F^- + 64H^+ + 66\ e^- \tag{9}$$
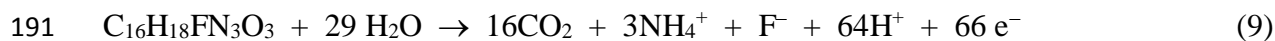
The specific energy consumption per unit TOC mass (EC_{TOC}) at time t (in h) for each trial was

calculated from Eq. (10) [18]:

$$EC_{TOC}\ (\text{kWh (g TOC)}^{-1})\ = \frac{E_{\text{cell}}\ I\ t}{V_s\ \triangle(\text{TOC})_{\text{exp}}} \tag{10}$$

where E_{cell} is the average cell voltage (in V).

The primary by-products formed in 3 L of 0.103 mM NFX, both in the 15 mM NaCl + 45 mM

Na_2SO_4 mixture and in 50 mM Na_2SO_4, employing 0.40 mM Fe^{2+} at $j = 15$ mA cm^{-2} were detected

by LC-MS/MS. A Thermo Fisher Scientific system composed of an Ultimate 3000 HPLC fitted with

a Phenomenex Luna 2.5 um C18-HST, 100 mm $\times$ 2.0 mm (i.d.), column at 40 °C, coupled to a LTQ-

Orbitrap Velos and an Accela PDA, was used. The mobile phase contained two components: A (H_2O)

and B (acetonitrile), both with 0.1% formic acid. The elution gradient was made by increasing the

composition of component B from 0% to 35% in 30 min and then, it was held 2 min to be returned to

0% in 30 min. The flow rate was 0.2 mL min^{-1}. On the other hand, stable intermediates accumulated

at 15 and 120 min of electrolysis in the mentioned mixture were identified by GC-MS using an Agilent Technologies system following our previously established procedure [16]. Two columns, a polar HP INNOWax and a non-polar Teknokroma Sapiens-X5ms, both of 0.25 μm, 30 m × 0.25 mm (i.d.), were used for a thorough analysis.

The acute toxicity of the urban wastewater effluent, spiked with NFX and treated by SPEF-HClO process, was determined as the concentration that effectively causes a reduction of 50% in the bioluminescence intensity of *Vibrio fischeri* marine bacteria after 15 min of exposure to the given sample, at 25 ºC. This allowed obtaining the so-called EC_{50} values in mg L^{-1}, using an AFNOR T90-301 Microtox system. The bacteria and required reagents were supplied by Modern Water, and the analysis was performed according to the standard Microtox test. Each sample had to be conditioned before analysis: (i) At the end of the electrolysis, the pH was increased to 10 and the resulting suspension was filtered with a 0.45 µm filter, thus removing the precipitated iron(III) hydroxide; (ii) the residual chlorine was destroyed by adding some drops of a 3% $Na_2S_2O_8$ solution; (iii) the resulting sample was adjusted to pH 7.3 and diluted prior to measurement.

3. Results and discussion

3.1. Comparative degradation of norfloxacin by different EAOPs with a Ti|Ir-Sn-Ru oxides anode

The first trials were made to compare the degradation and mineralization profiles when treating 3 L of 0.103 mM NFX solutions, containing 15 mM NaCl + 45 mM Na_2SO_4 at pH 3.0 and 30 ºC, by AO-HClO and EF-HClO (both in the dark), PEF-HClO under UVA light and SPEF-HClO. In all cases, a Ti|Ir-Sn-Ru oxides anode and a stainless-steel cathode were employed, operating at $j = 15$ mA cm^{-2} for 300 min. The three electrochemical Fenton-like processes were carried out upon addition of Fe^{2+} as homogeneous catalyst, at a concentration of 0.40 mM. Fig. 2a, which depicts the decay of normalized NFX concentration, highlights that the AO-HClO treatment was the fastest, achieving the total degradation in about 15 min, whereas a longer time close to 30 min was required in the three

Fenton-like treatments. All the degradation profiles agreed well with a pseudo-first-order kinetics, as clearly evidenced by the excellent linear correlations obtained (see the inset in Fig. 2a). Table 1 summarizes a decrease of the corresponding pseudo-first-order rate constants (k_1) values according to the sequence: AO-HClO (0.200 min^{-1}) >> SPEF-HClO (0.127 min^{-1}) > EF-HClO (0.104 min^{-1}) ≈ PEF-HClO (0.096 min^{-1}). This means that the electrochemical Fenton-like processes are less powerful than AO-HClO, which is not the usual behavior [5,18,21]. A second finding from Fig. 2a is the positive effect of sunlight, justifying the superiority of SPEF-HClO over EF-HClO and PEF-HClO. According to these trends, Fig. 2b highlights that the greatest mineralization of 53% in 300 min was achieved by AO-HClO, although the value was similar to 46-49% TOC removal attained for EF-HClO and SPEF-HClO, which in turn were more effective than PEF-HClO (40% abatement). It is remarkable that the largest mineralization rate in AO-HClO was reached during the first 30 min of electrolysis, suggesting the fast generation of very stable chloroderivatives. In contrast, a much slower TOC abatement can be observed for the other three processes, which can be attributed to a much lower accumulation of such chloroderivatives because of the parallel oxidation with $^{\bullet}$OH formed from reaction (4). The MCE values calculated for the four treatments are found in Fig. 2c. As expected, higher values were determined for AO-HClO, although the efficiency drastically fall down to attain a final value of 6.0% at 300 min, slightly superior to 4.0-5.7% obtained for the other treatments (see Table 1). Worth noting, considering the corresponding EC_{TOC} values given in Fig. 2d, one can conclude that the SPEF-HClO process was more cost-effective for mineralization, even surpassing AO-HClO (0.75 vs. 0.80 kWh (g TOC)$^{-1}$ at 300 min, see Table 1), potentially being a more attractive treatment in practice.

The larger degradation and mineralization achieved in AO-HClO with the 15 mM NaCl + 45 mM Na$_2$SO$_4$ solution is certainly indicative of a high generation of HClO at the Ti|Ir-Sn-Ru oxides anode from reactions (2) and (3), showing this oxidant a large ability to destroy NFX and its by-products, although yielding more recalcitrant chloroderivatives. The low production of physisorbed

11

253   M(•OH) with this anode from reaction (1) then seems to have an insignificant role in the destruction

254   of the drug. In addition, as was mentioned above, NFX has a particular structure related to the

255   presence of a carboxyl group, which seems to play an important role in the oxidation process. The

256   lower mineralization reached in the Fe^{2+}-catalyzed treatments can be attributed to the increased

257   refractoriness of NFX upon the formation of complexes with iron ions, especially with Fe^{3+} produced

258   from reaction (4). Moreover, the poorer oxidation ability of EF-HClO makes in evidence a strong

259   reduction of HClO concentration in the presence of Fe^{2+} from reaction (4), continuously regenerated

260   by reaction (5), with the alternative formation of •OH that attacks more slowly the drug and its

261   intermediates. This explains the slower TOC removal observed for EF-HClO as compared to AO-

262   HClO. The additional production of •OH from the photolytic reaction (6) in PEF-HClO does not seem

263   to contribute substantially to the overall degradation. The superiority of SPEF-HClO can be related

264   to a much greater photolytic •OH generation by reaction (6), as result of the higher power of the

265   incident sunlight. Despite this positive action of sunlight, the fact that no greater TOC abatement is

266   reached in the latter process can be associated to a large formation of chloroderivatives, with low

267   production of final short-chain carboxylic acids that are known to form Fe(III)-carboxylate complexes

268   easy to oxidize via reaction (7).

269   *3.2. Effect of experimental parameters on the performance of the SPEF-HClO process*

270   The goal of subsequent experiments was to assess the influence of several key variables in the

271   SPEF-HClO treatment of NFX in a 15 mM NaCl + 45 mM Na_2SO_4 synthetic solution at pH 3.0 and

272   30 °C. The change of the normalized drug content operating at *j* values ranging between 5 and 20 mA

273   cm^{-2}, when treating solutions containing 0.103 mM NFX and 0.40 mM Fe^{2+}, is presented in Fig. 3a.

274   As can be seen, a higher *j* value caused a faster degradation due to the greater generation of HClO

275   from the acceleration of Cl^- oxidation by reaction (2), with the concomitant enhancement of reaction

276   (3). As a result, total drug abatement was achieved at >120, 60, 30 and 15 min upon use of increasing

277   *j* values from 5 to 20 mA cm^{-2}. From the good pseudo-first-order kinetic analysis shown in the inset

12

278   of Fig. 3a, it was found that the k_1-values progressively grew from 0.020 min^{-1} at 5 mA cm^{-2} to 0.195

279   min^{-1} at 20 mA cm^{-2} (see Table 1), in agreement with the expected gradually greater HClO production.

280   In contrast, TOC was poorly destroyed under these conditions. Fig. 3b reveals a quicker TOC

281   abatement when j raised from 5 to 15 mA cm^{-2}, but with lower mineralization power at 20 mA cm^{-2}.

282   This loss of oxidation ability could be ascribed to two main factors: (i) the greater accumulation of

283   recalcitrant chloroderivatives at too high j, eventually inhibiting the mineralization process, and (ii)

284   the promotion of HClO destruction to yield ClO_3^- and ClO_4^- ions from reactions (11) and (12)

285   [10,12,23]. The first hypothesis seems more reasonable because a quite low ClO_3^- concentration was

286   determined in this treatment, as will be discussed below.

287    $HClO + 2H_2O \rightarrow ClO_3^- + 5H^+ + 4e^-$ (11)

288    $ClO_3^- + H_2O \rightarrow ClO_4^- + 2H^+ + 2e^-$ (12)

289   Results of Fig. 3b indicate that the best j-value for the SPEF-HClO process was 15 mA cm^{-2}.

290   This behavior can be corroborated from the data depicted in Fig. 3c and 3d, since the highest MCE

291   and the lowest EC_{TOC} values were attained under such conditions, respectively (see also Table 1).

292   The optimum $j = 15$ mA cm^{-2} was then chosen for the subsequent experiments. It is noticeable the

293   gradual TOC removal with time in SPEF-HClO, a distinct trait as compared to the drastic decay in

294   AO-HClO (see Fig. 2b and 3b). This corroborates the slower generation of chloroderivatives in the

295   former, which is accompanied by a drastic decay of MCE (see Fig. 3c) and a rise of EC_{TOC} (see Fig.

296   3d) as the electrolysis was prolonged.

297   Since Fe^{2+} catalyzes the destruction of electrogenerated HClO from reaction (4), and the resulting

298   Fe^{3+} may complex with NFX, the influence of the catalyst concentration on the SPEF-HClO

299   performance was further considered. Fig. 4a depicts a progressive decay in the degradation rate when

300   treating 0.103 mM drug solutions at the optimum $j = 15$ mA cm^{-2} upon increase of the Fe^{2+}

301   concentration from 0.10 to 0.50 mM, attaining total removal at about 20 to 45 min at the two extreme

302   Fe^{2+} concentrations. Again, the inset of this figure highlights that all concentration decays followed

a pseudo-first-order kinetics, with the corresponding k_1-values gradually decreasing from 0.132 min^{-1} at 0.10 mM Fe^{2+} to 0.078 min^{-1} at 0.50 mM Fe^{2+} (see Table 1). This loss of reactivity can then be associated with a greater loss of HClO as the Fe^{2+} content was risen because of the acceleration of reaction (4). In addition, owing to the carboxyl substituent in the NFX structure, a larger amount of stable Fe(III)-NFX complexes can take place [26], leading to a slower degradation kinetics at higher Fe^{2+} concentration. Conversely, when the TOC abatement was measured (see Fig. 4b), only 17% mineralization was reached at 0.10 mM Fe^{2+}, suggesting a greater formation of recalcitrant chloroderivatives from the higher quantities of HClO present in the medium. Note also that similar TOC decays were observed at catalyst concentrations above 0.1 mM, contrary to the behavior observed in previous works [22,24]. This is attributed to the consumption of iron ions to form complexes with the NFX, thereby decreasing the $^\bullet OH$ production via reaction (4), not being possible to have a progressively larger mineralization. Nonetheless, the highest mineralization of 43% was achieved at 0.40 mM Fe^{2+}, when the action of reactive $^\bullet OH$ formed from reactions (4) and (6) to mineralize the drug and its by-products was more remarkable. From the MCE and EC_{TOC} values depicted in Fig. 4c and 4d, respectively, one can infer again that the best Fe^{2+} concentration of the process is 0.40 mM, because it yielded a slightly higher MCE of 5.7% and lower EC_{TOC} of 0.75 kWh (g TOC)$^{-1}$. This Fe^{2+} concentration was selected for the following trials.

The effect of the initial NFX concentration between 0.051 and 1.46 mM was finally studied, at pH 3.0 and 30 ºC, operating with the optimum Fe^{2+} content (0.40 mM) and j (15 mA cm^{-2}). Fig. 5a shows that a longer time from 10 to >30 min was needed for overall drug disappearance in the presence of more NFX molecules. This slower degradation is expected if a similar amount of HClO and $^\bullet OH$ encounters a higher organic load. This behavior agrees with the decreasing k_1-values from 0.278 to 0.075 min^{-1} found from the kinetic analysis presented in the inset of Fig. 5a. The higher amount of HClO that attacks the lowest NFX content (0.051 mM) originates more rapidly a greater quantity of chloroderivatives, giving rise to a smaller TOC abatement, as can be seen in Fig. 5b. This

figure also shows a similar percentage of TOC abatement for 0.103 and 0.146 mM NFX, evidencing a larger oxidation ability of the system for the highest drug concentration. This can be observed in Fig. 5c and 5d, where higher MCE and lower EC_{TOC} values can be observed at 0.146 mM NFX, attaining final values of 7.0% and 0.63 kWh (g TOC)$^{-1}$ at 300 min, respectively. This means that the SPEF-HClO process becomes more efficient and cost-effective with increasing drug concentration.

3.3. Effect of the BDD anode

To check the oxidation ability of the M($^{\bullet}$OH) formed from reaction (1), the Ti|Ir-Sn-Ru oxides anode of the flow cell was replaced by a BDD thin film. It is well known that BDD is much more powerful because it produces a larger quantity of the above physisorbed radical [5,44,45]. The positive action of this anode on the degradation of 3 L of 0.103 mM NFX solutions containing 15 mM NaCl + 45 mM Na$_2$SO$_4$ and 0.40 mM Fe^{2+} at pH 3.0 and 30 ºC can be observed in Fig. 6a. About 15 min at *j*-values of 15 and 20 mA cm^{-2} were required to remove the drug, a time much shorter than 30 min determined for Ti|Ir-Sn-Ru (see Fig. 3a). Table 1 shows that higher k_1-values of 0.242 and 0.144 min^{-1} at 15 and 20 mA cm^{-2}, respectively, were calculated using the BDD anode. This behavior can then be related to a faster destruction of the drug by the high amount of BDD($^{\bullet}$OH) produced by BDD. Such enhancement of the oxidation power of the system can also justify the greater mineralization achieved with BDD, approaching 60% as shown Fig. 6b. This suggests a smaller accumulation of the recalcitrant chloroderivatives with this anode because of their faster oxidation by BDD($^{\bullet}$OH), which is more effective than M($^{\bullet}$OH) produced by the Ti|Ir-Sn-Ru oxides anode.

The positive effect of the BDD anode was obviously reflected in the MCE and EC_{TOC} values illustrated in Fig.6c and 6d, respectively. For example, at *j* = 15 mA cm^{-2}, the final MCE with this anode was 7.5%, much higher than 5.7% determined with Ti|Ir-Sn-Ru (see Table 1), as expected from its greater mineralization power. In contrast, the final EC_{TOC} value of 0.73 kWh (g TOC)$^{-1}$ calculated with BDD was only slightly lower than 0.75 kWh (g TOC)$^{-1}$ found with Ti|Ir-Sn-Ru, as a result of the higher E_{cell} value using the former anode (6.0 vs. 4.7 V). Consequently, the use of a BDD anode

353 yielded a quicker degradation of NFX and enhanced its mineralization, although requiring a similar

354 energy consumption.

355 Worth noticing, worse results have been reported by Carneiro et al. [46] for the treatment 1 L of

356 solutions containing 100 mg L^{-1} NFX + 0.1 M NaCl, using a flow system with a filter-press cell

357 equipped with a BDD anode operating at $j = 10$ mA cm^{-2}. Total degradation was more slowly achieved

358 (i.e., 60 min), whereas a similar TOC decay of about 60% was attained in 300 min. In contrast, Özcan

359 et al. [49] described the total disappearance of 0.25 mM of NFX, with total TOC removal in 150 min,

360 by EF process with a BDD/carbon felt cell at 300 mA, using 175 mL of stirred solutions with 0.05 M

361 Na_2SO_4 + 0.1 mM Fe^{3+} at pH 3.0. The absence of Cl^- in the medium is thus critical for ensuring the

362 mineralization of NFX solutions because no recalcitrant chloroderivatives are formed.

363 *3.4. Degradation in WWTP effluent*

364 The study of the SPEF-HClO treatment of NFX solutions was extended to an actual water matrix.

365 This aqueous solution exhibited a complex composition with organic compounds like natural organic

366 matter (NOM) associated to humic and fulvic acids, and a mixture of inorganic ions with high

367 contents of Cl^- (10.2 mM) and SO_4^{2-} (1.50 mM) ions (see subsection 2.2). Although the amount of

368 Cl^- was slightly lower than in the synthetic solution tested above (15 mM), it was high enough to

369 produce significant quantities of HClO from reaction (3), allowing an efficient removal of the drug.

370 This fact can be observed in Fig. 7a which depicts the comparative normalized drug concentration

371 decay when treating 3 L of 0.103 mM drug solutions in the WWTP effluent and in the 15 mM NaCl

372 + 45 mM Na_2SO_4 synthetic solution by SPEF-HClO. In both cases, 0.40 mM Fe^{2+} was added as

373 catalyst after adjusting the pH to 3.0, and a $j = 15$ mA cm^{-2} was applied using the Ti|Ir-Sn-Ru anode.

374 The drug abatement was a bit slower in the WWTP effluent due to the parallel oxidation of its organic

375 components, although NFX completely disappeared in 30 min, i.e., the same time as in the synthetic

376 matrix. The inset of Fig. 7a reveals that the decay in the WWTP effluent obeyed a pseudo-first-order

377 kinetics, with a lower k_1-value of 0.078 min^{-1} (see Table 1).

16

378   Regarding the corresponding TOC abatement of the above trials presented in Fig. 7b, one can

379   deduce that the percentage of TOC removal also decreased more slowly in the WWTP effluent as

380   compared to that in the synthetic solution (40% vs. 46% at 300 min). However, considering the

381   superior initial TOC of the former medium (31 vs. 20 mg L^{-1}), it can be concluded that a larger amount

382   of TOC is actually removed (12.4 vs. 9.2 mg L^{-1}). That means that 3.2 mg L^{-1} TOC of the initial

383   WWTP effluent were additionally mineralized during the SPEF-HClO treatment, demonstrating the

384   high power of this procedure to partially destroy its organic components. Despite this positive fact,

385   the lower conductivity of this matrix as compared to that of the synthetic solution resulted in a greater

386   E_{cell} (9.1 vs. 4.4 V), thus requiring a higher energy consumption for the mineralization process. In

387   agreement, Fig.7c shows a higher EC_{TOC} using the WWTP effluent as compared to the synthetic

388   solution, with final values of 1.21 and 0.75 kWh (g TOC)$^{-1}$, respectively. These findings disclose the

389   good effectiveness of the SPEF-HClO process to remediate WWTP effluents contaminated with

390   NFX, being the energy consumption affected by a lower conductivity.

391   *3.5. Time-course of reactive species and final products*

392   The evolution of the reactive species HClO was determined during the AO-HClO treatment

393   (without Fe^{2+}) of 3 L of both the 15 mM NaCl + 45 mM Na$_2$SO$_4$ synthetic solution and the WWTP

394   effluent, at pH 3.0, 30 °C and $j = 15$ mA cm^{-2}. Fig. 8a depicts a continuous accumulation of the oxidant

395   in the synthetic medium up to reach a steady value of 1.42 mM after 240 min of electrolysis. The

396   achievement of this steady state could be related to the equilibrium between HClO generation from

397   reaction (4) and its destruction to form ClO$_3^-$ and ClO$_4^-$ ions from reactions (11) and (12). In contrast,

398   Fig. 8b makes in evidence that in the WWTP effluent, HClO was always continuously accumulated,

399   reaching a higher content of 4.0 mM at 300 min. Under these conditions, the organic components of

400   the wastewater are competitively oxidized on the anode, suggesting the minimization of HClO

401   oxidation to ClO$_3^-$ and ClO$_4^-$ ions to finally favor its greater accumulation.

402   The variation of the concentrations of Fe^{2+} and Fe_{total} with electrolysis time was assessed under

403   SPEF-HClO conditions without the drug, employing 3 L of the synthetic solution or the WWTP

404   effluent, always with 0.40 mM Fe^{2+} at pH 3.0 and 30 ºC, operating at $j = 15$ mA cm^{-2}. Fig. 8c shows

405   a steady loss of about 63% of Fe^{2+} from 120 min of electrolysis in the synthetic medium, suggesting

406   a faster reaction of this ion with electrogenerated HClO during that time to form Fe^{3+} ion, whereupon

407   its disappearance is counterbalanced by the regeneration of Fe^{2+} from Fe^{3+} reduction via reaction (5).

408   In the WWTP effluent, Fig. 8e reveals the existence of a more complex behavior, with a similar rapid

409   loss of 58% of Fe^{2+} for 120 min, probably due to its fast reaction with HClO that is accelerated by

410   the consumption of $^{\bullet}$OH formed from reaction (4) in the oxidation of its organic components. The

411   subsequent decay of Fe^{2+} content to 79% until 240 min is probably due to an enhancement of such

412   organic oxidation, whereas the subsequent drop of this oxidation could decrease the rate of reaction

413   (5) and increase the accumulation of Fe^{3+} giving rise to a final loss of 64%. The above evolution of

414   Fe^{2+} is also reflected in that of Fe_{total} present in each medium. As can be seen in Fig. 8d for the

415   synthetic medium, near 20% of Fe_{total} disappeared after 300 min of electrolysis, suggesting its

416   precipitation as $Fe(OH)_3$ that can explain part of the loss of Fe^{2+} shown in Fig. 8c. A higher removal

417   of Fe_{total} can be seen in Fig. 8f using the WWTP effluent, which achieved a value as high as 55% at

418   300 min, suggesting again a large influence of organic oxidation to accelerate reaction (4) that favors

419   the generation of an excess of Fe^{3+} that promotes its precipitation as $Fe(OH)_3$. This agrees with the

420   higher loss of Fe^{2+} in the WWTP effluent as compared to that in the synthetic matrix, as depicted in

421   Fig. 8e.

422   The evolution of different species formed during the NFX mineralization was determined for the

423   SPEF-HClO treatment of 3 L of 0.260 mM drug in the synthetic solution with 0.40 mM Fe^{2+} at pH

424   3.0, 30 ºC and $j = 15$ mA cm^{-2}. Fig. 9a highlights the profile of formic acid that was the only final

425   short-chain linear aliphatic carboxylic acid detected by ion-exclusion HPLC. This product was

426   gradually accumulated up to 1.223 mM at 120 min, further decreasing down to 0.539 mM at 300 min.

427   This final value accounts for 6.5 mg L^{-1} of TOC, i.e., 23.2% of the residual TOC in the treated solution

428   (28 mg L^{-1}). Such decay can be explained by the photolysis of the formed Fe(III)-formate complexes

429   via reaction (7), directly originating Fe^{2+} and CO$_2$ [16,17]. Note that formic acid has also been

430   detected during the mineralization of NFX by other AOPs, such as catalytic ozonation with

431   MnO$_x$/SBA-15 [54] and peroxymonosulfate activated with nanosized magnetic CuFe$_2$O$_4$ [55]. In both

432   cases, oxalic and acetic acids could be identified as well, but they did not appear under the SPEF-

433   HClO conditions tested here.

434   Since the NFX molecules contain F and N as heteroatoms, their release as F$^-$ and NH$_4^+$ ions

435   during the SPEF-HClO treatment was monitored. As can be seen in Fig. 9b, the F$^-$ concentration was

436   continuously accumulated up to 0.211 mM, which represents a loss of 81% of the initial F content.

437   That means that 19% of the initial F remained as fluoroderivatives at the end of the electrolysis. Fig.

438   9c shows the accumulation of a very low and steady amount of NH$_4^+$ of 0.0225 mM almost during

439   the whole electrolysis. Considering that the initial N content in the drug was 0.780 mM, its

440   transformation into NH$_4^+$ only account for 3.3%, a value much lower than that obtained for the F$^-$

441   release. This suggests a large formation of volatile N$_x$O$_y$ by-products, a common feature in the

442   destruction of N-compounds by electrochemical Fenton-based processes [53,56].

443   The loss of 3.0 mM Cl$^-$ with the production of 0.44 mM ClO$_3^-$ after 300 min of the above SPEF-

444   HClO treatment is shown in Fig. 9d. The decay of Cl$^-$ concentration in the synthetic matrix can be

445   ascribed to different phenomena: (i) the release from the medium of volatile Cl$_2$ gas formed from

446   reaction (2), expected to be a minor route because the pH was not sufficiently acid in the bulk; (ii)

447   the production of HClO from reaction (4) (see Fig. 8a); and (iii) the formation of chloroderivatives

448   from the attack of HClO over the drug and its intermediates. The detection of ClO$_3^-$ during the process

449   corroborates the destruction of HClO by reactions (11) and (12) under the conditions tested.

450   *3.6. Reaction sequence for norfloxacin degradation*

451   Table 2 collects 10 primary by-products identified by LC-MS/MS analysis during the treatment

452   of 3 L of 0.103 mM NFX (**1**) in both, a 15 mM NaCl + 45 mM Na_2SO_4 synthetic solution by SPEF-

453   HClO and a 50 mM Na_2SO_4 solution by AO, always with a Ti|Ir-Sn-Ru oxides anode and 0.40 mM

454   Fe^{2+}, at pH 3.0, 30 ºC and j = 15 mA cm^{-2} for 300 min. The study with 50 mM Na_2SO_4 was performed

455   to better detect the by-products originated by $^\bullet OH$ and M($^\bullet OH$). These by-products involve the

456   hydroxylation followed by the oxidation of the piperazine ring (compounds **2**, **5**, **6**, **7**, and **8**), the

457   chlorination of the naphthalene ring (compounds **3** and **9**), and defluorination (compounds **4**, **10**, and

458   **11**). Note that compounds **8** and **9** have also been reported as by-products of **1** during its

459   electrochemical chlorination [48] or AO in different wastewater matrices [47].

460   Based on the above derivatives, the initial reaction sequence for **1** degradation is proposed in Fig.

461   10, involving three parallel paths via compounds **2**, **3**, and **4**. The first path is initiated by the attack

462   of $^\bullet OH$ on the C(3) of the piperazine group of **1** to yield the hydroxylated compound **2**, which is

463   converted into compound **5** with cleavage of the piperazine group or compound **6** with generation of

464   a carbonyl functionality in the C(2) position of this group. Further oxidation of both compounds **5**

465   and **6** originates compound **7** with two carbonyl groups linked to the two N atoms of the broken

466   piperazine group that further evolves to compound **8** with the loss of the carbonyl group linked to the

467   N atom bonded to the naphthalene ring. Note that these degradation by-products were also found by

468   Chen et al. [35]. The second path corresponds to the starting chlorination over the C(9) of the

469   naphthalene ring of **1** to form compound **3**, followed by the cleavage and loss of the piperazine group

470   to produce compound **9**. The third path starts with the hydroxylation in the C(7) position of the

471   naphthalene group with release of a F^- ion to yield compound **4**. The subsequent cleavage of the

472   naphthalene ring of **4** yields compound **10**, which is then hydroxylated and decarboxylated to form

473   compound **11**.

474   Table 3 lists 5 stable by-products identified by GC-MS detected after 15 and 120 min of the

475   above SPEF-HClO trial. These by-products are formed from the degradation of the aforementioned

476 primary by-products and are four N-derivatives (compounds **12**-**15**), along with formic acid (**16**), also

477 detected by ion-exclusion HPLC (see Fig. 9a). In the literature, the formation of compounds **13** and

478 **16** has been reported from the NFX destruction by chlorine dioxide [40] and EF [49], respectively.

479 *3.7. Evolution of the acute toxicity*

480 As discussed above, the appearance of some by-products (e.g., chlorinated compounds) could

481 potentially cause an increase in the solution toxicity during its treatment. Therefore, a toxicity analysis

482 was carried out during the electrolysis of 3 L of the WWTP effluent containing 0.103 mM NFX + 0.4

483 mM Fe^{2+} at pH 3.0 by SPEF-HClO, using the solar flow plant shown in Fig.1 at $j = 15$ mA cm^{-2} and

484 LFR = 180 L h^{-1} for 300 min. Fig. 11 shows that the initial toxicity value (i.e., once the NFX was spiked

485 into the wastewater), in terms of EC_{50}, was 49 mg L^{-1}. Along the electrolysis, the toxicity remained

486 almost constant during the first 240 min (i.e., EC_{50} of 53 mg L^{-1}), which suggests the formation of by-

487 products with a similar toxicity for the fluorescent bacteria [57,58]. Conversely, the solution became

488 much less toxic toward the end of the treatment, reaching a final EC_{50} of 91.3 mg L^{-1}. This is indicative

489 of the disappearance of the more toxic by-products, as for example the chlorinated compounds **3** and **9**

490 detected during the first 40 min, or compounds **4** and **5**, despite the fact that 60% of the initial TOC

491 remained in the WWTP effluent after its treatment [59]. Based on this, at industrial scale, the SPEF-

492 HClO process could be used to pre-treat the WWTP effluent, and the resulting solution could be further

493 conditioned by means of a post-biological post-treatment aimed at water reuse, at least for irrigation

494 purposes. This sequential method might be a suitable option for the treatment of a real WWTP effluent

495 contaminated with NFX and, probably, with other aromatic organics.

496 **4. Conclusions**

497 It has been shown that the AO-HClO treatment of NFX in a synthetic solution containing NaCl

498 and Na_2SO_4 at pH 3.0 with a Ti|Ir-Sn-Ru oxides anode becomes more efficient than the analogous

499 EF-HClO, PEF-HClO and SPEF-HClO treatments with 0.40 mM Fe^{2+}. The unexpected better

performance of AO-HClO is explained by: (i) the accumulation of higher amounts of electrogenerated HClO, which is partially converted into $^{\bullet}OH$ in the electrochemical Fenton-based treatments, and (ii) the formation of refractory Fe(III)-NFX complexes in the latter processes. AO-HClO only yielded a 53% TOC abatement due to the accumulation of stable chloroderivatives. In contrast, the good Fe^{2+} photoregeneration in SPEF-HClO allowed a gradual mineralization that could have more interest in practice. Optimum conditions for treating up to 0.146 mM NFX by SPEF-HClO were found: 0.40 mM Fe^{2+} and $j = 15$ mA cm^{-2}. The use of BDD anode accelerated the degradation and mineralization, although the calculated energy consumption was similar becasuwe of the higher E_{cell} as compared to Ti|Ir-Sn-Ru anode. A slower degradation was found for the SPEF-HClO process in the WWTP effluent due to the parallel oxidation of its organic components, but it was still effective. The mineralization process was accompanied by the production of formic acid and F^-, as well as minor amounts of NH_4^+ and ClO_3^-. Up to 10 primary organic by-products involving hydroxylation, chlorination and defluorination of NFX have been identified by LC-MS/MS, allowing the proposal of its initial degradation sequence. Other 5 stable by-products formed during the SPEF-HClO treatment have been detected by GC-MS.

Acknowledgements

References

[1]   E.Y. Klein, T.P. Van Boeckel, E.M. Martínez, R. Laxminarayan, Global increase and geographic convergence in antibiotic consumption between 2000 and 2015, Proc Natl Acad Sci USA 115 (2018) E3463–E3470. https://doi-org.sire.ub.edu/10.1073/pnas.1717295115.

523   [2]   K. Kümmerer, The presence of pharmaceuticals in the environment due to human use –

524   present knowledge and future challenges, J. Environ. Manage. 90 (2009) 2354–2366.

525   https://doi.org/10.1016/j.jenvman.2009.01.023.

526   [3]   W.J. Sim, J.W. Lee, E.S. Lee, S.K. Shin, S.R. Hwang, J.E. Oh, Occurrence and distribution

527   of pharmaceuticals in wastewater from households, livestock farms, hospitals and

528   pharmaceutical manufactures, Chemosphere. 82 (2011) 179–186.

529   https://doi.org/10.1016/j.chemosphere.2010.10.026.

530   [4]   V. Homem, L. Santos, Degradation and removal methods of antibiotics from aqueous

531   matrices: A review, J. Environ. Manage. 92 (2011) 2304–2347.

532   https://doi.org/10.1016/j.jenvman.2011.05.023.

533   [5]   C.A. Martínez-Huitle, M.A. Rodrigo, I. Sirés, O. Scialdone, Single and coupled

534   electrochemical processes and reactors for the abatement of organic water pollutants: A

535   critical review, Chem. Rev. 115 (2015) 13362–13407.

536   https://doi.org/10.1021/acs.chemrev.5b00361.

537   [6]   S. Lanzalaco, I. Sirés, A. Galia, M.A. Sabatino, C. Dispenza, O. Scialdone, Facile crosslinking

538   of poly(vinylpyrrolidone) by electro-oxidation with IrO_2-based anode under potentiostatic

539   conditions, J. Appl. Electrochem. 48 (2018) 1343-1352. https://doi.org/10.1007/s10800-018-

540   1237-8.

541   [7]   F.C. Moreira, R.A.R. Boaventura, E. Brillas, V.J.P. Vilar, Electrochemical advanced

542   oxidation processes: A review on their application to synthetic and real wastewaters, Appl.

543   Catal. B: Environ. 202 (2017) 217–261. https://doi.org/10.1016/j.apcatb.2016.08.037.

544   [8]   O. Ganzenko, C. Trellu, N. Oturan, D. Huguenot, Y. Péchaud, E.D. van Hullebusch, M.A.

545   Oturan, Electro-Fenton treatment of a complex pharmaceutical mixture: Mineralization

546   efficiency and biodegradability enhancement, Chemosphere 253 (2020) 126659.

547   https://doi.org/10.1016/j.chemosphere.2020.126659.

548   [9]   V.B. Lima, L.A. Goulart, R.S. Rocha, J.R. Steter, M.R.V. Lanza, Degradation of antibiotic

549   ciprofloxacin by different AOP systems using electrochemically generated hydrogen

550   peroxide, Chemosphere 247 (2020) 125807.

551   https://doi.org/10.1016/j.chemosphere.2019.125807.

552   [10]   Y. Zhang, G. Daniel, S. Lanzalaco, A.A. Isse, A. Facchin, A. Wang, E. Brillas, C. Durante, I.

553   Sirés, H_2O_2 production at gas-diffusion cathodes made from agarose-derived carbons with

554   different textural properties for acebutolol degradation in chloride media, J. Hazard. Mater.

555   423 (2022) 127005. https://doi.org/10.1016/j.jhazmat.2021.127005.

556   [11]   M.F. Murrieta, J.L. Nava, Electrosynthesis of hypochlorous acid in a filter-press electrolyzer

557   and its modeling in dilute chloride solutions, J. Electroanal. Chem. 892 (2021) 115286.

558   https://doi.org/10.1016/j.jelechem.2021.115286.

559   [12]   O. Scialdone, F. Proietto, A. Galia, Electrochemical production and use of chlorinated

560   oxidants for the treatment of wastewater contaminated by organic pollutants and disinfection,

561   Curr. Opin. Electrochem. 27 (2021) 100682. https://doi.org/10.1016/j.coelec.2020.100682.

562   [13]   M.R. Cruz-Díaz, E.P. Rivero, F.A. Rodríguez, R. Domínguez-Bautista, Experimental study

563   and mathematical modeling of the electrochemical degradation of dyeing wastewaters in

564   presence of chloride ion with dimensional stable anodes (DSA) of expanded meshes in a

565   FM01-LC reactor, Electrochim. Acta. 260 (2018) 726–737.

566   https://doi.org/10.1016/j.electacta.2017.12.025.

567   [14]   N. Kishimoto, E. Sugimura, Feasibility of an electrochemically assisted Fenton method using

568   Fe^{2+}/HOCl system as an advanced oxidation process, Water Sci. Technol. 62 (2010) 2321–

569   2329. https://doi.org/10.2166/wst.2010.203.

570   [15]   L.P. Candeias, M.R.L. Stratford, P. Wardman, Formation of hydroxyl radicals on reaction of

571   hypochlorous acid with ferrocyanide, a model iron(II) complex, Free. Rad. Res. 4 (1994) 241-

572   249. https://doi.org/10.3109/10715769409147520.

573 [16] G. Coria, I. Sirés, E. Brillas, J.L. Nava, Influence of the anode material on the degradation of

574 naproxen by Fenton-based electrochemical processes, Chem. Eng. J. 304 (2016) 817–825.

575 https://doi.org/10.1016/J.CEJ.2016.07.012.

576 [17] G. Coria, T. Pérez, I. Sirés, E. Brillas, J.L. Nava, Abatement of the antibiotic levofloxacin in

577 a solar photoelectro-Fenton flow plant: Modeling the dissolved organic carbon concentration-

578 time relationship, Chemosphere 198 (2018) 174–181.

579 https://doi.org/10.1016/j.chemosphere.2018.01.112.

580 [18] J.R. Steter, E. Brillas, I. Sirés, Solar photoelectro-Fenton treatment of a mixture of parabens

581 spiked into secondary treated wastewater effluent at low input current, Appl. Catal. B:

582 Environ. 224 (2018) 410–418. https://doi.org/10.1016/j.apcatb.2017.10.060.

583 [19] R. Salazar, J. Gallardo-Arriaza, J. Vidal, C. Rivera-Vera, C. Toledo-Neira, M.A. Sandoval, L.

584 Cornejo-Ponce, A. Thiam, Treatment of industrial textile wastewater by the solar

585 photoelectro-Fenton process: Influence of solar radiation and applied current, Sol. Energy.

586 190 (2019) 82–91. https://doi.org/10.1016/j.solener.2019.07.072.

587 [20] G. Daniel, Y. Zhang, S. Lanzalaco, F. Brombin, T. Kosmala, G. Granozzi, A. Wang, E. Brillas,

588 I. Sirés, C. Durante, Chitosan-derived nitrogen-doped carbon electrocatalyst for a sustainable

589 upgrade of oxygen reduction to hydrogen peroxide in UV-assisted electro-Fenton water

590 treatment, ACS Sustain. Chem. Eng. 8 (2020) 14425–14440.

591 https://dx.doi.org/10.1021/acssuschemeng.0c04294.

592 [21] I. Sirés, E. Brillas, Upgrading and expanding the electro-Fenton and related processes, Curr.

593 Opin. Electrochem. 27 (2021) 100686. https://doi.org/10.1016/j.coelec.2020.100686.

594 [22] M.F. Murrieta, I. Sirés, E. Brillas, J.L. Nava, Mineralization of Acid Red 1 azo dye by solar

595 photoelectro-Fenton-like process using electrogenerated HClO and photoregenerated Fe(II),

596 Chemosphere 246 (2020) 125697. https://doi.org/10.1016/j.chemosphere.2019.125697.

597   [23]   Z.G. Aguilar, E. Brillas, M. Salazar, J.L. Nava, I. Sirés, Evidence of Fenton-like reaction with

598   active chlorine during the electrocatalytic oxidation of Acid Yellow 36 azo dye with Ir-Sn-Sb

599   oxide anode in the presence of iron ion, Appl. Catal. B: Environ. 206 (2017) 44–52.

600   https://doi.org/10.1016/j.apcatb.2017.01.006.

601   [24]   M.F. Murrieta, E. Brillas, J.L. Nava, I. Sirés, Photo-assisted electrochemical production of

602   HClO and Fe^{2+} as Fenton-like reagents in chloride media for sulfamethoxazole degradation,

603   Sep. Purif. Technol. 250 (2020) 117236. https://doi.org/10.1016/j.seppur.2020.117236.

604   [25]   D.A.C. Coledam, I. Sánchez-Montes, B.F. Silva, J.M. Aquino, On the performance of

605           $HOCl/Fe^{2+}$, $HOCl/Fe^{2+}/UVA$, and HOCl/UVC processes using in situ electrogenerated active

606   chlorine to mineralize the herbicide picloram, Appl. Catal. B: Environ. 227 (2018) 170–177.

607   https://doi.org/10.1016/j.apcatb.2017.12.072.

608   [26]   F. Gozzi, I. Sirés, S.C. de Oliveira, A. Machulek, E. Brillas, Influence of chelation on the

609   Fenton-based electrochemical degradation of herbicide tebuthiuron, Chemosphere 199 (2018)

610   709–717. https://doi.org/10.1016/j.chemosphere.2018.02.060.

611   [27]   I. Sirés, E. Guivarch, N. Oturan, M.A. Oturan, Efficient removal of triphenylmethane dyes

612   from aqueous medium by in situ electrogenerated Fenton's reagent at carbon-felt cathode,

613   Chemosphere 72 (2008) 592–600. https://doi.org/10.1016/j.chemosphere.2008.03.010.

614   [28]   Y.Q. Hu, S. Zhang, Z. Xu, Z.S. Lv, M.L. Liu, L.S. Feng, 4-Quinolone hybrids and their

615   antibacterial activities, Eur. J. Med. Chem. 141 (2017) 335–345.

616   https://doi.org/10.1016/j.ejmech.2017.09.050.

617   [29]   K.S. Shreenidhi, P. Priyavadhana, N. Purnima, A. Rashminiza, S. Sneha, B. Vijaya Geetha,

618   Study on the toxic effects of pharmaceutical drugs – Norfloxacin using *Pangasius Sp.* fish

619   model and its mitigation using *Artemisia pallens*, Acta Ecol. Sin. (2022).

620   https://doi.org/10.1016/j.chnaes.2021.08.014.

621 [30] M. Gros, M. Petrović, D. Barceló, Development of a multi-residue analytical methodology

622 based on liquid chromatography-tandem mass spectrometry (LC-MS/MS) for screening and

623 trace level determination of pharmaceuticals in surface and wastewaters, Talanta 70 (2006)

624 678–690. https://doi.org/10.1016/j.talanta.2006.05.024.

625 [31] C. Yang, X. Wang, L. Zhang, W. Dong, C. Yang, X. Shi, Y. Fan, Y. Wang, H. Lv, W. Wang,

626 Y. Zhao, Investigation of kinetics and mechanism for the degradation of antibiotic norfloxacin

627 in wastewater by UV/H$_2$O$_2$, J. Taiwan Inst. Chem. Eng. 115 (2020) 117–127.

628 https://doi.org/10.1016/j.jtice.2020.09.036.

629 [32] J. Liu, G. Lu, D. Wu, Z. Yan, A multi-biomarker assessment of single and combined effects

630 of norfloxacin and sulfamethoxazole on male goldfish (*Carassius auratus*), Ecotox. Environ.

631 Safe. 102 (2014) 12–17. https://doi.org/10.1016/j.ecoenv.2014.01.014.

632 [33] X.L. Zhao, P. Li, S.Q. Zhang, S.W. He, S.Y. Xing, Z.H. Cao, R. Lu, Z.H. Li, Effects of

633 environmental norfloxacin concentrations on the intestinal health and function of juvenile

634 common carp and potential risk to humans, Environ. Pollut. 287 (2021) 117612.

635 https://doi.org/10.1016/j.envpol.2021.117612.

636 [34] M. Chen, W. Chu, H$_2$O$_2$ assisted degradation of antibiotic norfloxacin over simulated solar

637 light mediated Bi$_2$WO$_6$: Kinetics and reaction pathway, Chem. Eng. J. 296 (2016) 310–318.

638 https://doi.org/10.1016/j.cej.2016.03.083.

639 [35] M. Chen, W. Chu, Photocatalytic degradation and decomposition mechanism of

640 fluoroquinolones norfloxacin over bismuth tungstate: Experiment and mathematic model,

641 Appl. Catal. B: Environ. 168–169 (2015) 175–182.

642 https://doi.org/10.1016/j.apcatb.2014.12.023.

643 [36] X. Jin, X. Zhou, P. Sun, S. Lin, W. Cao, Z. Li, W. Liu, Photocatalytic degradation of

644 norfloxacin using N-doped TiO$_2$: Optimization, mechanism, identification of intermediates

645   and toxicity evaluation, Chemosphere 237 (2019) 124433.

646   https://doi.org/10.1016/j.chemosphere.2019.124433.

647   [37] H. Mohan, M. Ramasamy, V. Ramalingam, K. Natesan, M. Duraisamy, J. Venkatachalam, T.

648   Shin, K.K. Seralathan, Enhanced visible light-driven photocatalysis of iron-oxide/titania

649   composite: Norfloxacin degradation mechanism and toxicity study, J. Hazard. Mater. 412

650   (2021) 125330. https://doi.org/10.1016/j.jhazmat.2021.125330.

651   [38] A.L. Fornazaria, V.F. Labriola, B.F. da Silva, L.F. Castro, J.R. Perussi, E.M. Vieira, E.B.

652   Azevedo, Coupling Zero-Valent Iron and Fenton processes for degrading sulfamethazine,

653   sulfathiazole, and norfloxacin, J. Environ. Chem. Eng. 9 (2021) 105761.

654   https://doi.org/10.1016/j.jece.2021.105761.

655   [39] C. Wang, G. Yu, H. Chen, J. Wang, Degradation of norfloxacin by hydroxylamine enhanced

656   Fenton system: Kinetics, mechanism and degradation pathway, Chemosphere 270 (2021).

657   https://doi.org/10.1016/j.chemosphere.2020.129408.

658   [40] R. Su, L. Huang, N. Li, L. Li, B. Jin, W. Zhou, B. Gao, Q. Yue, Q. Li, Chlorine dioxide

659   radicals triggered by chlorite under visible-light irradiation for enhanced degradation and

660   detoxification of norfloxacin antibiotic: Radical mechanism and toxicity evaluation, Chem.

661   Eng. J. 414 (2021) 128768. https://doi.org/10.1016/j.cej.2021.128768.

662   [41] J. Lu, J. Li, J. Xu, H. Tang, Z. Lv, E. Du, L. Wang, M. Peng, Kinetics, structural effects and

663   transformation pathways for norfloxacin oxidation using the UV/chlorine process, J. Water

664   Process. Eng. 44 (2021) 102324. https://doi.org/10.1016/j.jwpe.2021.102324.

665   [42] L. Chen, X. Zuo, S. Yang, T. Cai, D. Ding, Rational design and synthesis of hollow

666   Co_3O_4@Fe_2O_3 core-shell nanostructure for the catalytic degradation of norfloxacin by

667   coupling with peroxymonosulfate, Chem. Eng. J. 359 (2019) 373–384.

668   https://doi.org/10.1016/j.cej.2018.11.120.

669 [43] X. Chen, R. Zhuan, J. Wang, Assessment of degradation characteristic and mineralization

670 efficiency of norfloxacin by ionizing radiation combined with Fenton-like oxidation, J.

671 Hazard. Mater. 404 (2021) 124172. https://doi.org/10.1016/j.jhazmat.2020.124172.

672 [44] D.A.C. Coledam, J.M. Aquino, B.F. Silva, A.J. Silva, R.C. Rocha-Filho, Electrochemical

673 mineralization of norfloxacin using distinct boron-doped diamond anodes in a filter-press

674 reactor, with investigations of toxicity and oxidation by-products, Electrochim. Acta. 213

675 (2016) 856–864. https://doi.org/10.1016/j.electacta.2016.08.003.

676 [45] J. Mora-Gomez, E. Ortega, S. Mestre, V. Pérez-Herranz, M. García-Gabaldón,

677 Electrochemical degradation of norfloxacin using BDD and new Sb-doped SnO_2 ceramic

678 anodes in an electrochemical reactor in the presence and absence of a cation-exchange

679 membrane, Sep. Purif. Technol. 208 (2019) 68–75.

680 https://doi.org/10.1016/j.seppur.2018.05.017.

681 [46] J.F. Carneiro, J.M. Aquino, B.F. Silva, A.J. Silva, R.C. Rocha-Filho, Comparing the

682 electrochemical degradation of the fluoroquinolone antibiotics norfloxacin and ciprofloxacin

683 using distinct electrolytes and a BDD anode: evolution of main oxidation byproducts and

684 toxicity, J. Environ. Chem. Eng. 8 (2020) 104433. https://doi.org/10.1016/j.jece.2020.104433.

685 [47] S.D. Jojoa-Sierra, J. Silva-Agredo, E. Herrera-Calderon, R.A. Torres-Palma, Elimination of

686 the antibiotic norfloxacin in municipal wastewater, urine and seawater by electrochemical

687 oxidation on IrO_2 anodes, Sci. Total. Environ. 575 (2017) 1228–1238.

688 https://doi.org/10.1016/j.scitotenv.2016.09.201.

689 [48] E.A. Serna-Galvis, S.D. Jojoa-Sierra, K.E. Berrio-Perlaza, F. Ferraro, R.A. Torres-Palma,

690 Structure-reactivity relationship in the degradation of three representative fluoroquinolone

691 antibiotics in water by electrogenerated active chlorine, Chem. Eng. J. 315 (2017) 552–561.

692 https://doi.org/10.1016/j.cej.2017.01.062.

[49] A. Özcan, A. Atılır Özcan, Y. Demirci, Evaluation of mineralization kinetics and pathway of norfloxacin removal from water by electro-Fenton treatment, Chem. Eng. J. 304 (2016) 518–526. https://doi.org/10.1016/j.cej.2016.06.105.

[50] D. Yu, J. He, Z. Wang, H. Pang, L. Li, Y. Zheng, Y. Chen, J. Zhang, Mineralization of norfloxacin in a CoFe–LDH/CF cathode-based heterogeneous electro-Fenton system: Preparation parameter optimization of the cathode and conversion mechanisms of H_2O_2 to $\cdot OH$, Chem. Eng. J. 417 (2021) 129240. https://doi.org/10.1016/j.cej.2021.129240.

[51] APWA, AWWA, WEF, Method number 4500-Cl Chlorine (residual)-G. DPD colorimetric method, in: Standard Methods for the Examination of Water and Wastewater, American Public Health Association, Washington D.C, USA, 2005, pp. 4-67–4-68.

[52] AWWA, AWWA, WEF, Fe^{2+} content from the red complex formed with 1,10-phenantroline, in: Standard Methods for the Examination of Water and Wastewater, American Public Health Association, Washington D.C, USA, 2005, pp. 3-77–3-79.

[53] R. Oriol, D. Clematis, E. Brillas, J.L. Cortina, M. Panizza, I. Sirés, Groundwater treatment using a solid polymer electrolyte cell with mesh electrodes, ChemElectroChem 6 (2019) 1235–1243. https://doi.org/10.1002/celc.201801906.

[54] W. Chen, X. Li, Z. Pan, S. Ma, L. Li, Synthesis of MnO_x/SBA-15 for norfloxacin degradation by catalytic ozonation, Sep. Purif. Technol. 173 (2017) 99-104. https://doi.org/10.1016/j.seppur.2016.09.030.

[55] Y. Wang, D. Tian, W. Chu, M. Li, X. Lu, Nanoscaled magnetic $CuFe_2O_4$ as an activator of peroxymonosulfate for the degradation of antibiotics norfloxacin, Sep. Purif. Technol. 212 (2019) 536-544. https://doi.org/10.1016/j.seppur.2018.11.051.

[56] A. Thiam, E. Brillas, J.A. Garrido, R.M. Rodríguez, I. Sirés, Routes for the electrochemical degradation of the artificial food azo-colour Ponceau 4R by advanced oxidation processes, Appl. Catal. B: Environ. 180 (2016) 227–236. http://dx.doi.org/10.1016/j.apcatb.2015.06.039.

718 [57] A. Tegze, G. Sági, K. Kovács, R. Homlok, T. Tóth, C. Mohácsi-Farkas, L. Wojnárovits, E.

719 Takács, Degradation of fluoroquinilone antibiotics during ionizing radiation treatment and

720 assessment of antibacterial activity, toxicity and biodegradability of the products, Radiat.

721 Phys. Chem. 147 (2018) 101-105. https://doi.org/10.1016/j.radphyschem.2018.02.015.

722 [58] M.T. Montañés, M. García-Gabaldón, Ll. Roca-Pérez, J.J. Giner-Sanz, J. Mora-Gómez, V.

723 Pérez-Herranz, Analysis of norfloxacin ecotoxicity and the relation with its degradation by

724 means of electrochemical oxidation using different anodes, Ecotoxicon. Environ. Saf. 188

725 (2020) 109923. https://doi.org/10.1016/j.ecoenv.2019.109923.

726 [59] X. Chen, J. Wang, Degradation of norfloxacin in aqueous solution by ionizing irradiation:

727 Kinetics, pathway and biological toxicity, Chem. Eng. J. 395 (2020) 125095.

728 https://doi.org/10.1016/j.cej.2020.125095.

Fig. 1. Sketch of the experimental setup of the solar flow plant used in this work.

Fig. 2. Variation of (a) normalized norfloxacin (NFX) concentration and kinetic analysis (inset), (b) normalized TOC, (c) mineralization current efficiency, and (d) energy consumption per unit TOC mass with electrolysis time for the treatment of 3 L of 0.103 mM (20 mg L^{-1} TOC) NFX in a synthetic solution with 15 mM NaCl + 45 mM Na_2SO_4 at pH 3.0 and 30 ℃ by AO-HClO, EF-HClO, PEF-HClO and SPEF-HClO. A flow plant like that of Fig. 1 was used, at current density (j) of 15 mA cm^{-2} and liquid flow rate (LFR) of 180 L h^{-1}. For the Fenton-based processes, 0.40 mM Fe^{2+} was added as catalyst. In PEF-HClO, the solution was recirculated through an annular photoreactor of 600 mL with an internal 160 W UVA lamp.

Fig. 3. Effect of j over the time course of (a) normalized NFX concentration and kinetic analysis (inset), (b) normalized TOC, (c) mineralization current efficiency, and (d) energy consumption per unit TOC mass for the SPEF-HClO treatment of 3 L of 0.103 mM NFX in a synthetic solution with 15 mM NaCl + 45 mM Na_2SO_4 and 0.40 mM Fe^{2+} at pH 3.0 and 30 ℃, using the solar flow plant of Fig. 1 at LFR = 180 L h^{-1}.

Fig. 4. Influence of Fe^{2+} content on (a) normalized NFX concentration and kinetic analysis (inset), (b) normalized TOC, (c) mineralization current efficiency, and (d) energy consumption per unit TOC mass vs. electrolysis time for the SPEF-HClO treatment at j = 15 mA cm^{-2}, under the conditions described in Fig. 3.

Fig. 5. Effect of the initial NFX content over the change of (a) normalized drug concentration and kinetic analysis (inset), (b) normalized TOC, (c) mineralization current efficiency, and (d) energy consumption per unit TOC mass with electrolysis time for the SPEF-HClO at j = 15 mA cm^{-2}, under the conditions described in Fig. 3.

Fig. 6. Influence of j in the SPEF-HClO process, under analogous conditions to those of Fig. 3 but using a BDD anode instead of the Ti|Ir-Sn-Ru oxides anode.

Fig. 7. Comparative variation of (a) normalized NFX concentration and kinetic analysis (inset), (b) normalized TOC, and (c) energy consumption per unit TOC mass with electrolysis time for the SPEF-HClO treatment of 3 L of 0.103 mM drug in a WWTP effluent (initial TOC = 31 mg L^{-1}) and in a synthetic solution with 15 mM NaCl + 45 mM Na_2SO_4 (initial TOC = 20 mg L^{-1}) at pH 3.0, 30 ℃, j = 15 mA cm^{-2} and LFR = 180 L h^{-1}, using the solar flow plant of Fig. 1 and 0.40 mM Fe^{2+}.

Fig. 8. Active chlorine concentration accumulated during the AO-HClO treatment of 3 L of (a) a 15 mM NaCl + 45 mM Na_2SO_4 synthetic solution and (b) a WWTP effluent, in both cases at pH 3.0, 30 ℃, j = 15 mA cm^{-2} and LFR = 180 L h^{-1}, using the solar flow plant of Fig. 1. Change of (c,e) normalized Fe^{2+} content and (d,f) normalized total Fe with electrolysis time for the SPEF-HClO trials of Fig. 7 in (c,d) the synthetic solution and (e,f) the WWTP effluent.

Fig. 9. Evolution of the concentrations of (a) formic acid, (b) fluoride ion, (c) ammonium ion, and (d) chloride and chlorate ions determined during the SPEF-HClO treatment of 3 L of 0.260 mM NFX in a synthetic solution with 15 mM NaCl + 45 mM Na_2SO_4 and 0.40 mM Fe^{2+} at pH 3.0 and 30 ℃, using the solar flow plant of Fig. 1 at j = 15 mA cm^{-2} and LFR = 180 L h^{-1}.

Fig. 10. Initial reaction sequence for the degradation of NFX at pH 3.0 by SPEF-HClO.

Fig. 11. Change of EC_{50} with time, with *Vibrio fischeri* as indicator organism, during the SPEF-HClO treatment of 3 L of WWTP effluent containing 0.103 mM NFX + 0.4 mM Fe^{2+} at pH 3.0, using the solar flow plant of Fig. 1 at j = 15 mA cm^{-2} and LFR = 180 L h^{-1}.

Fig. 1

Stainless steel cathode

Ti|Ir-Sn-Ru anode

Filter-press
FM01-LC
reactor

Heat exchangers

Solar planar
photoreactor

Power supply

3 L Reservoir

Rotameter

Pump
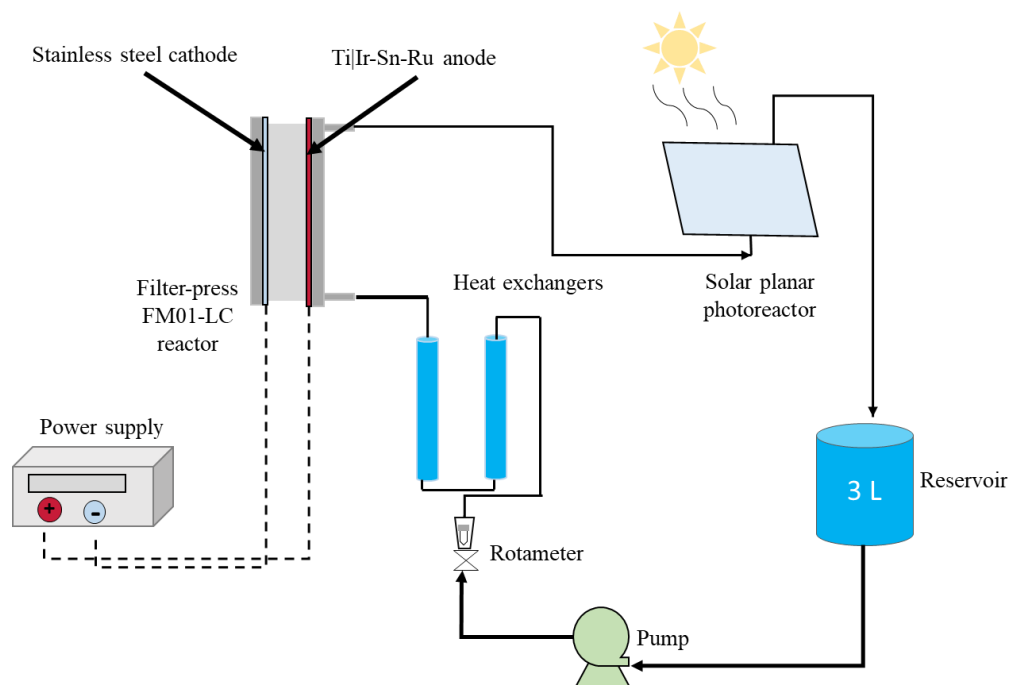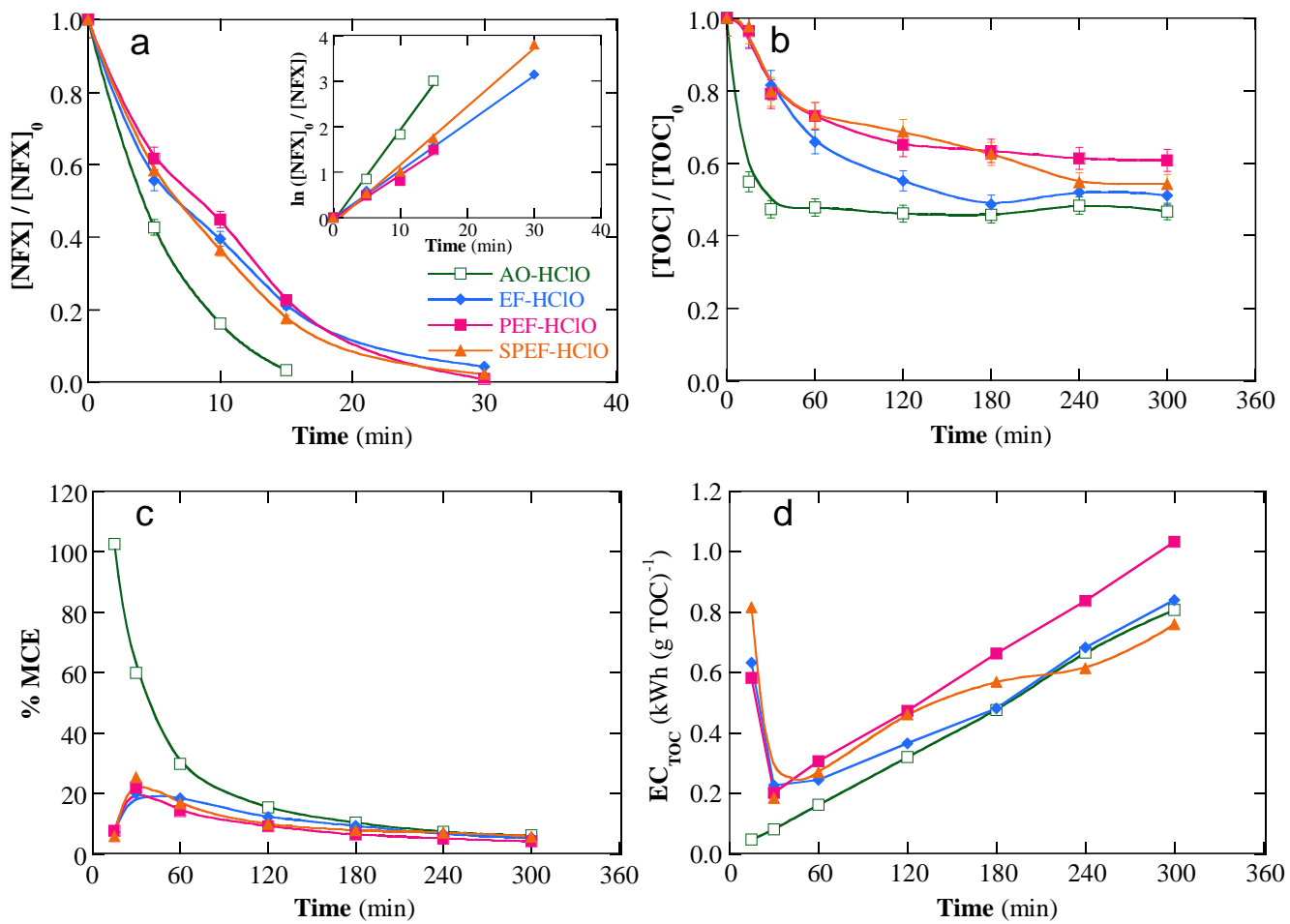
Fig. 2
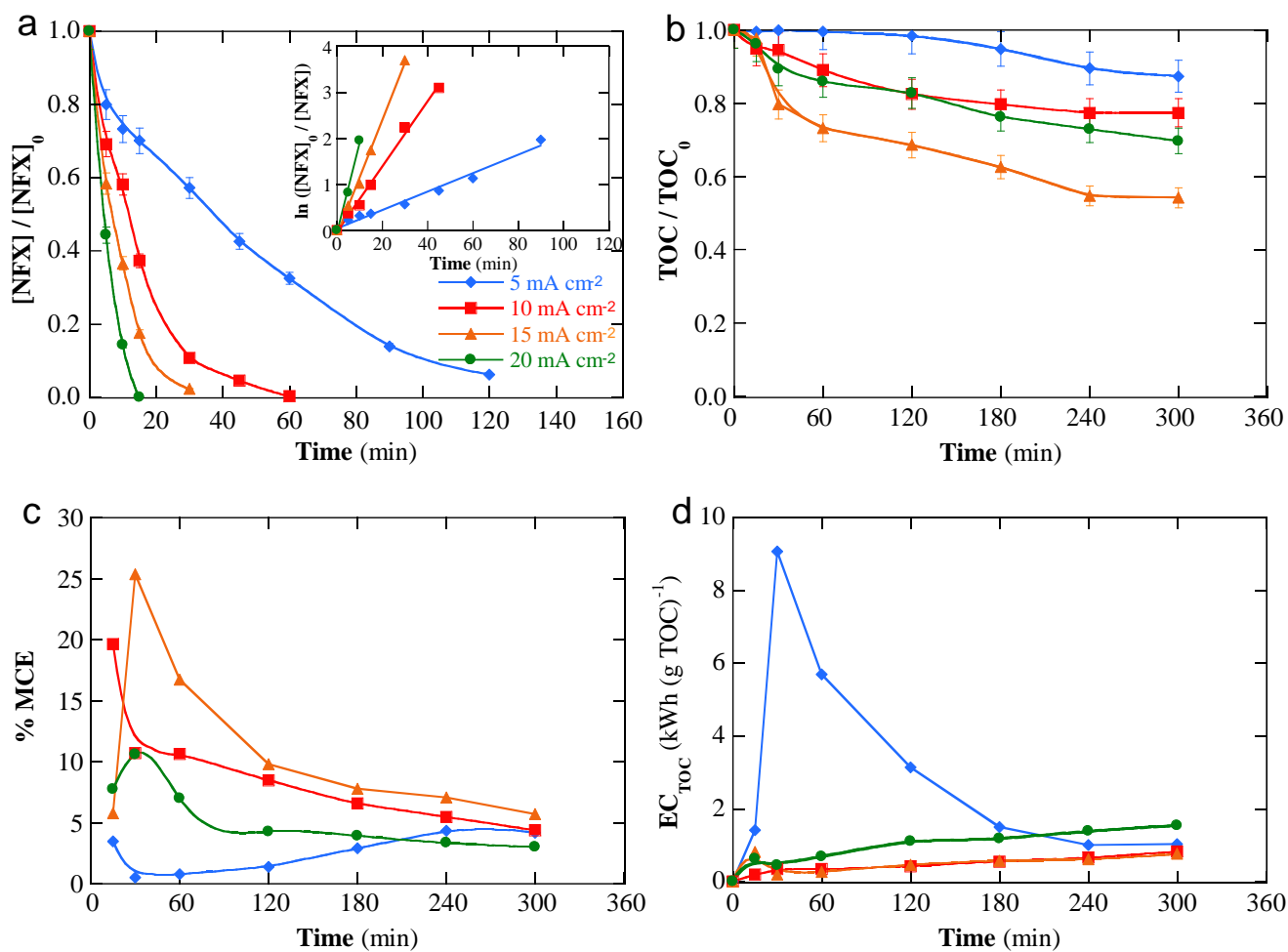
Fig. 3
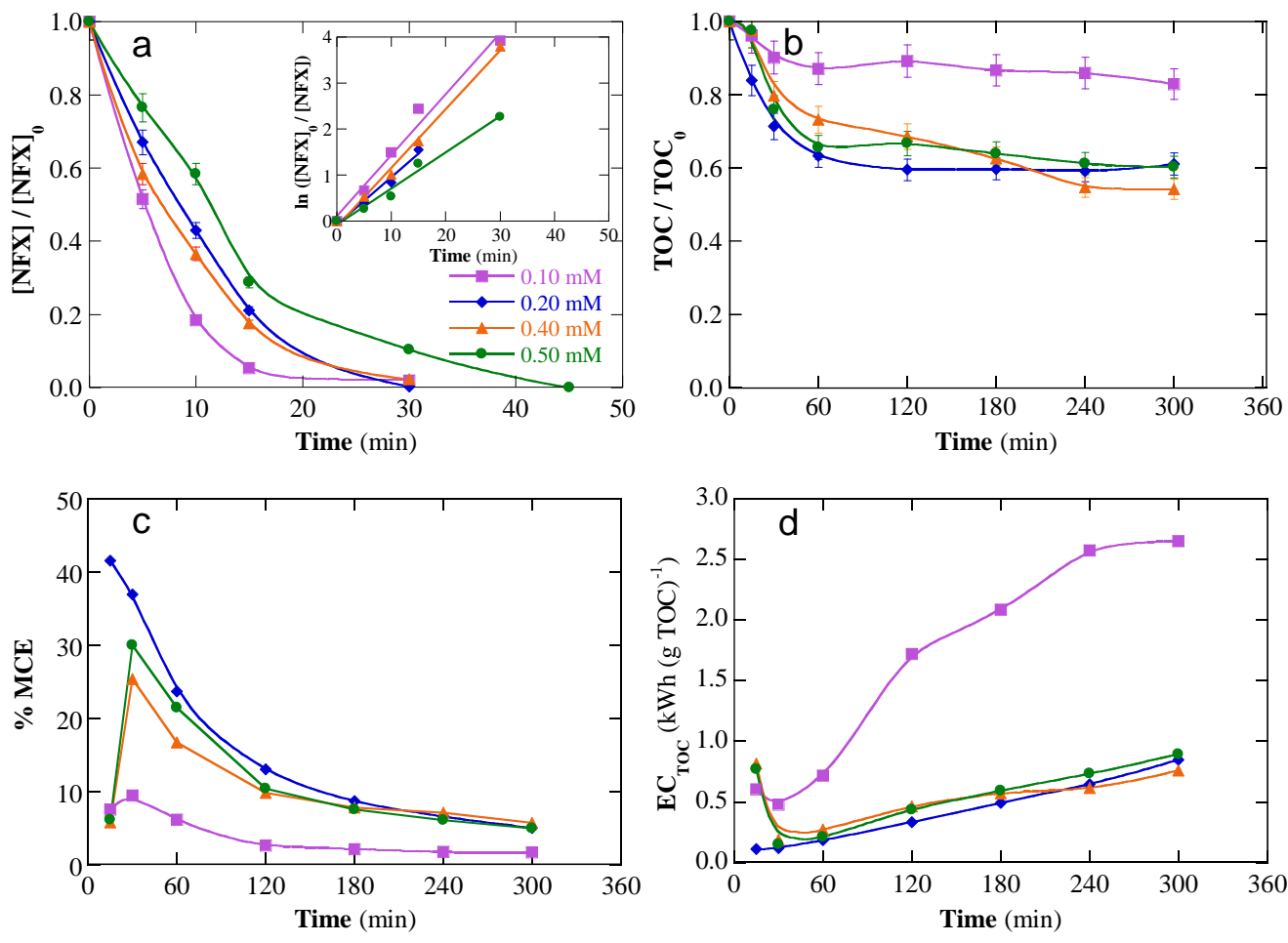
Fig. 4
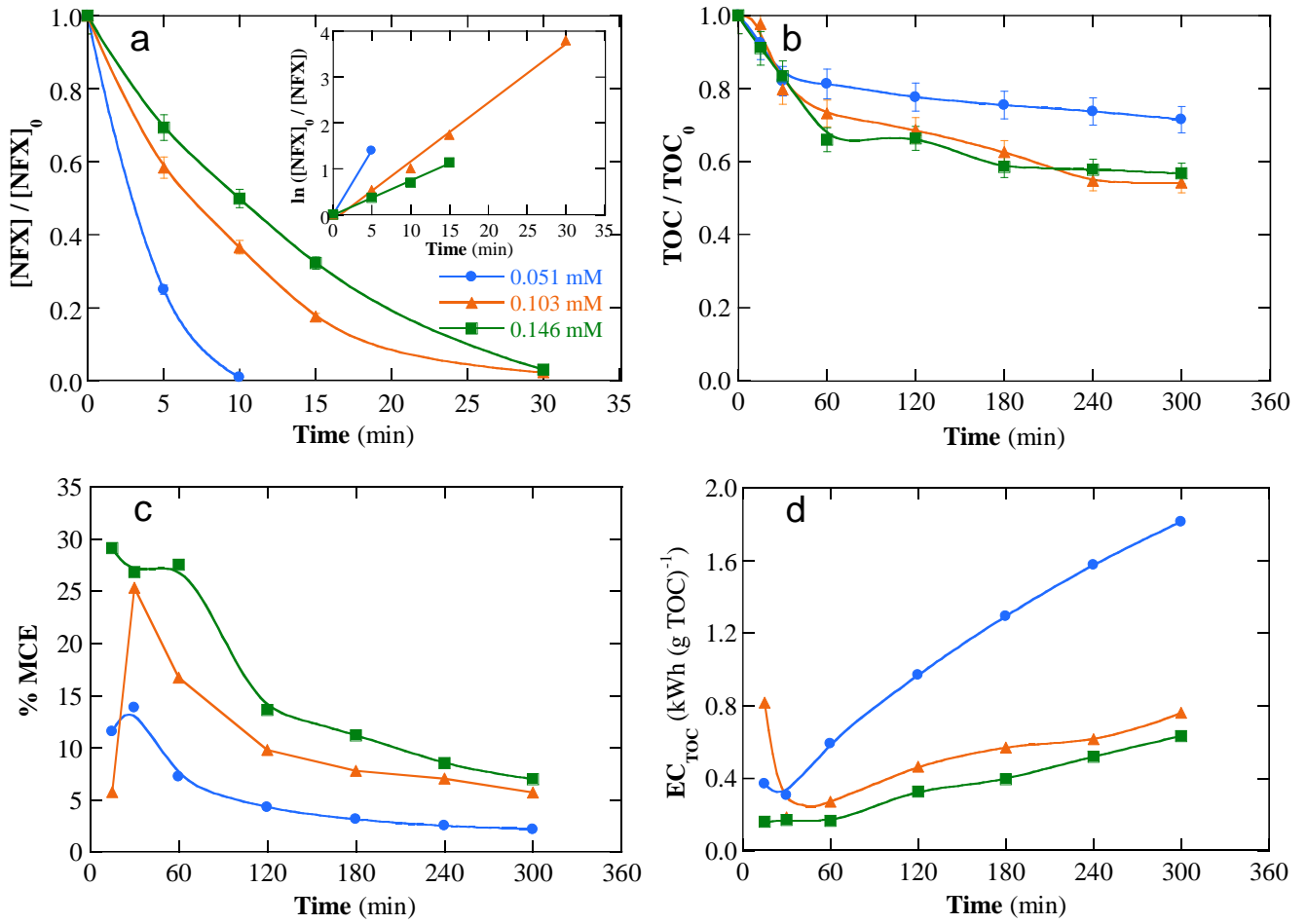
Fig. 5
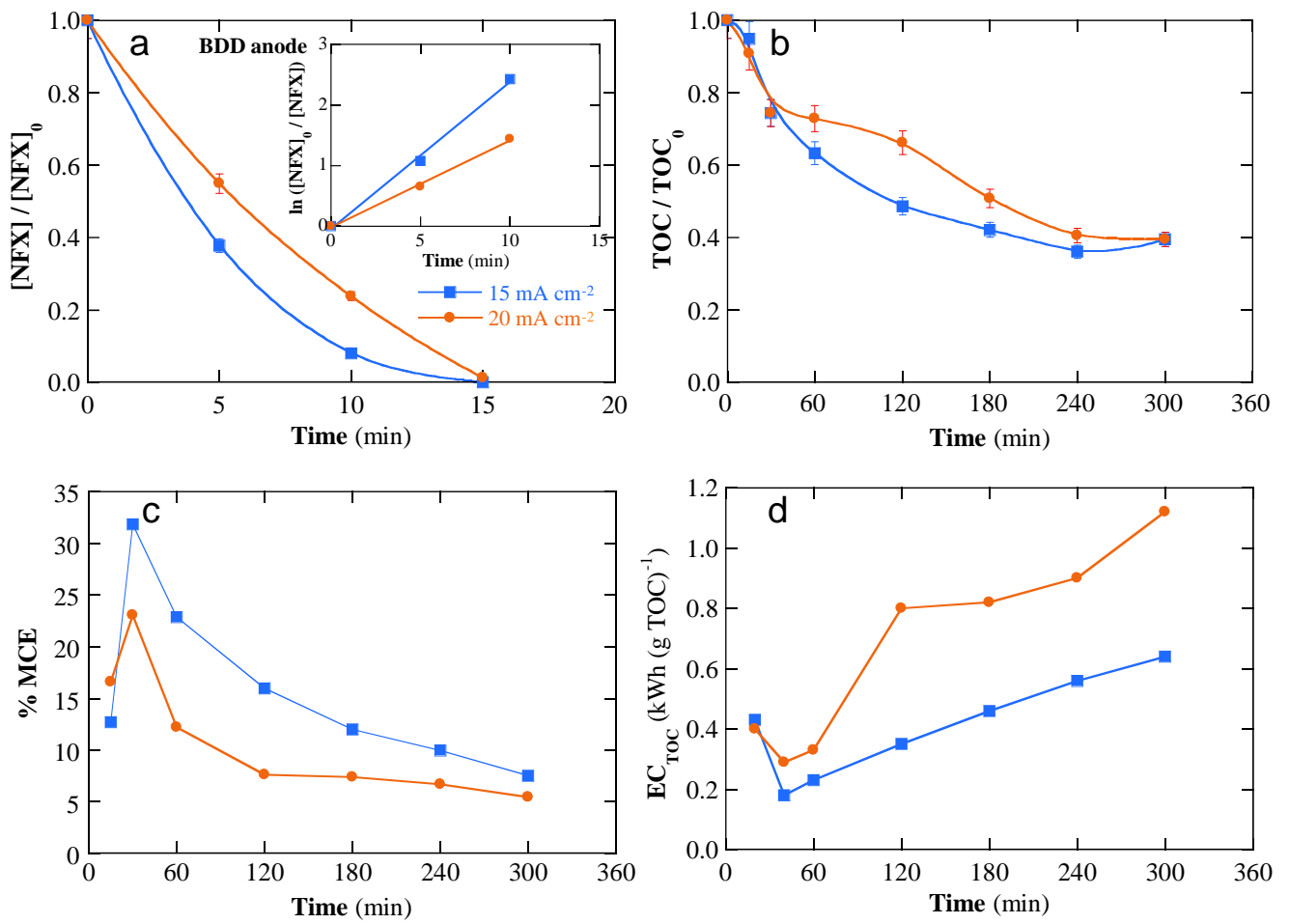
Fig. 6
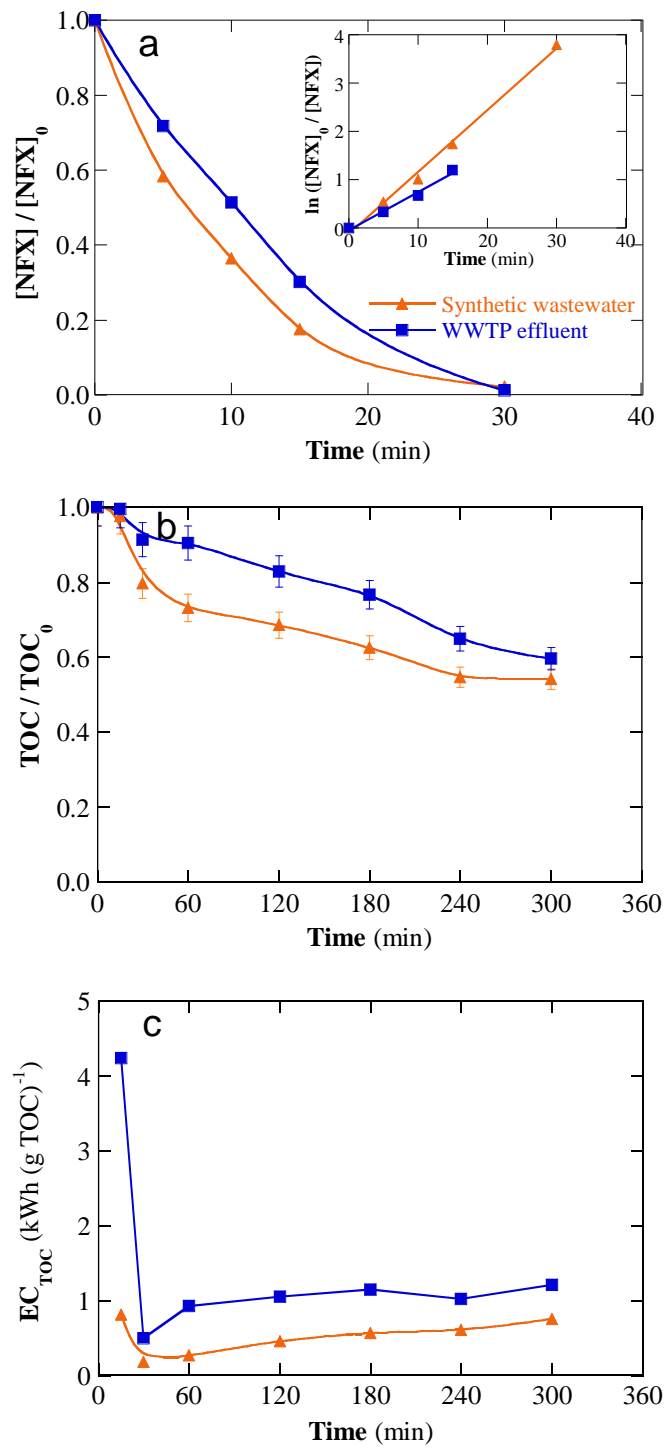
Fig. 7
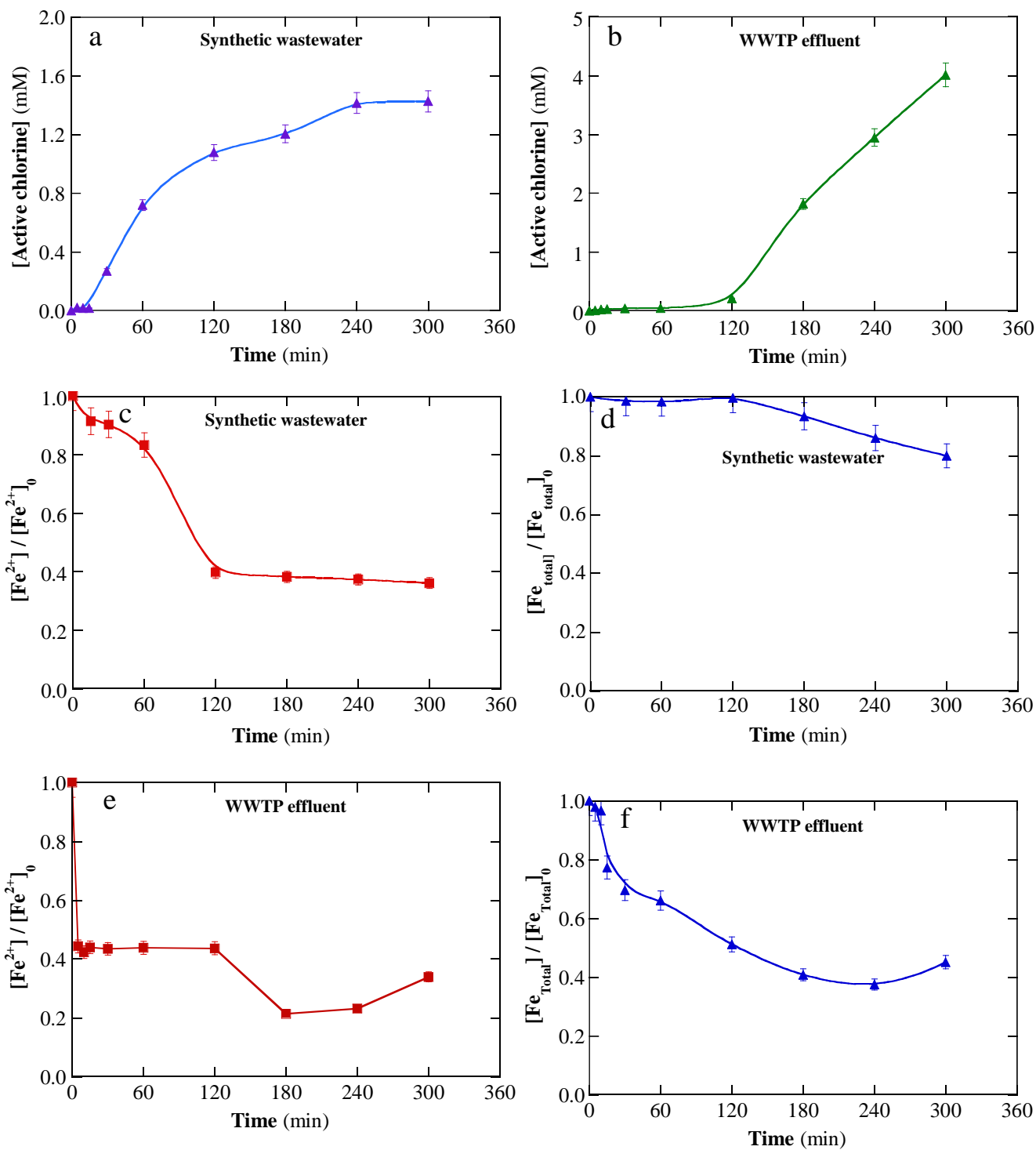
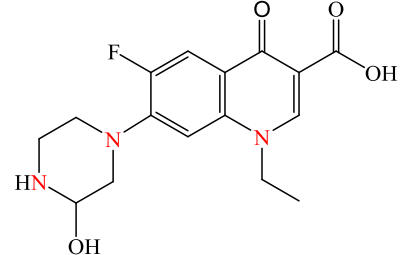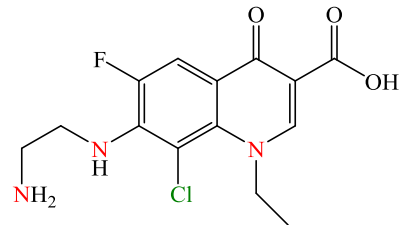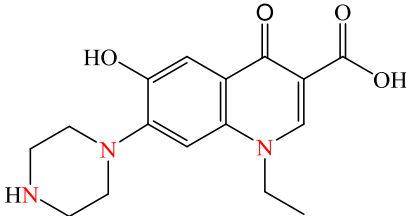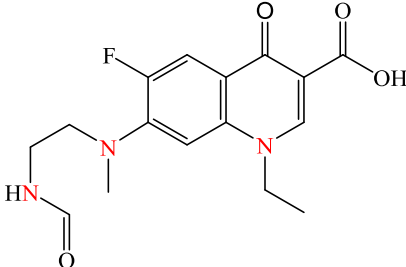**Fig. 8**
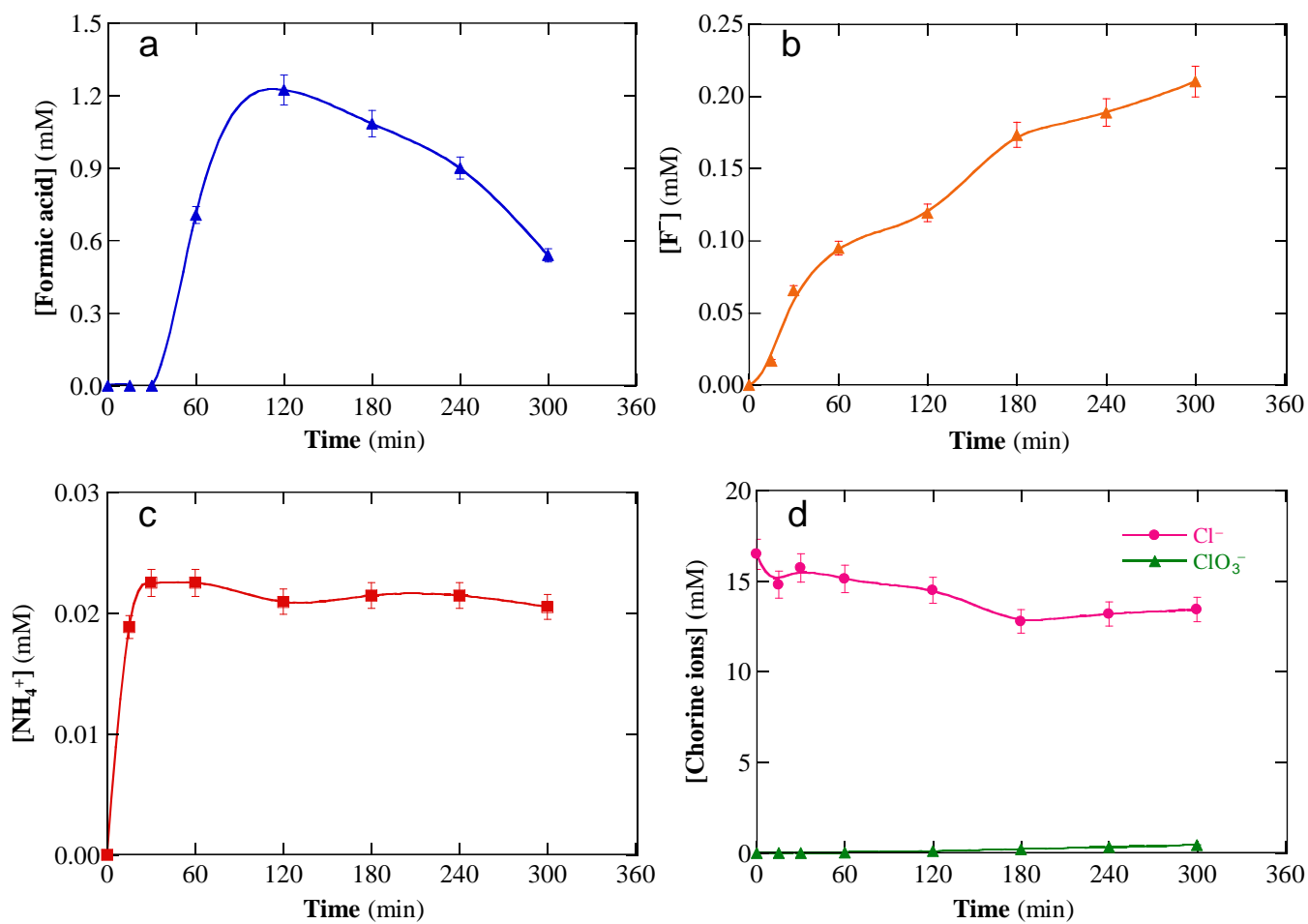
Fig. 9
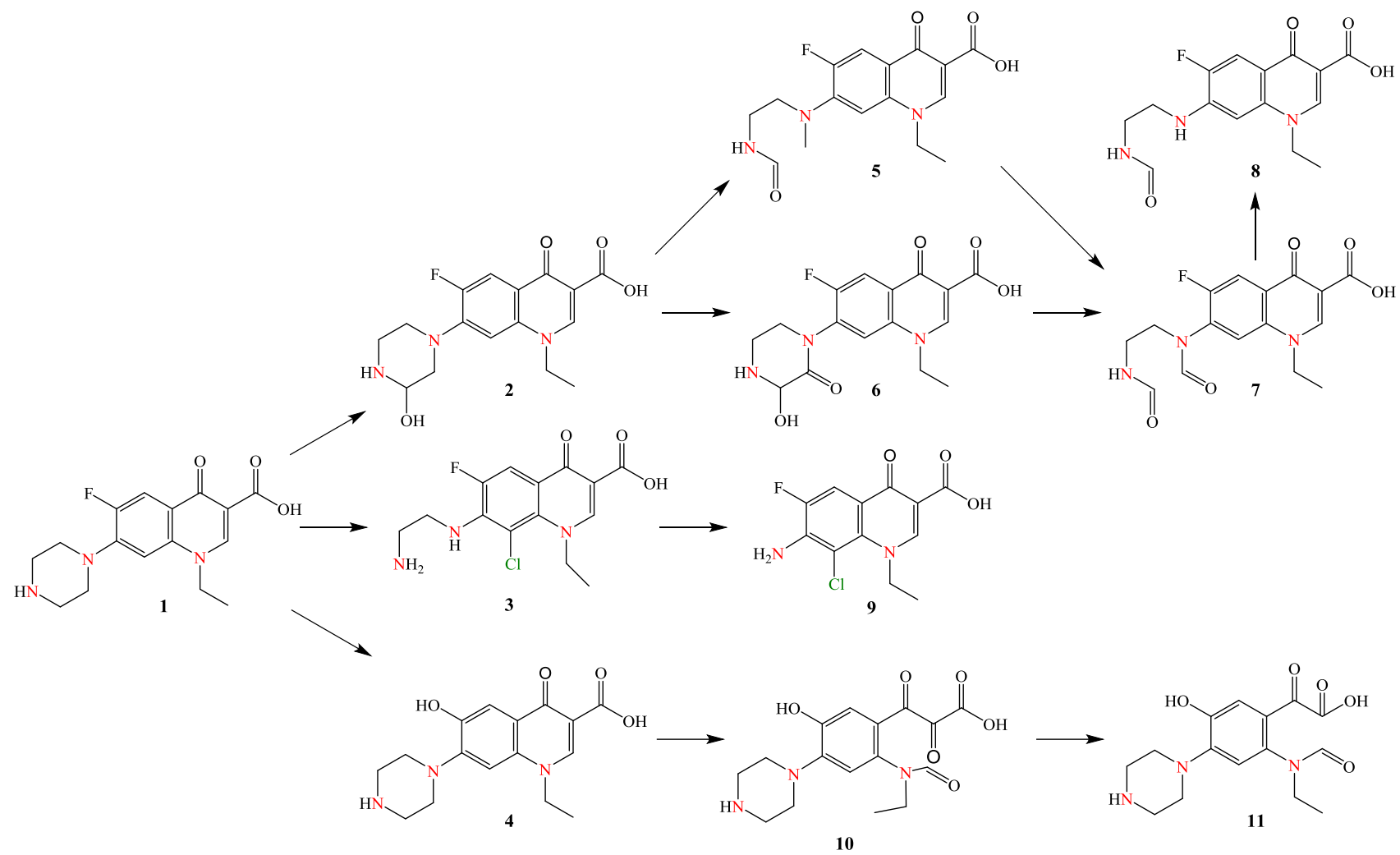
Fig. 10
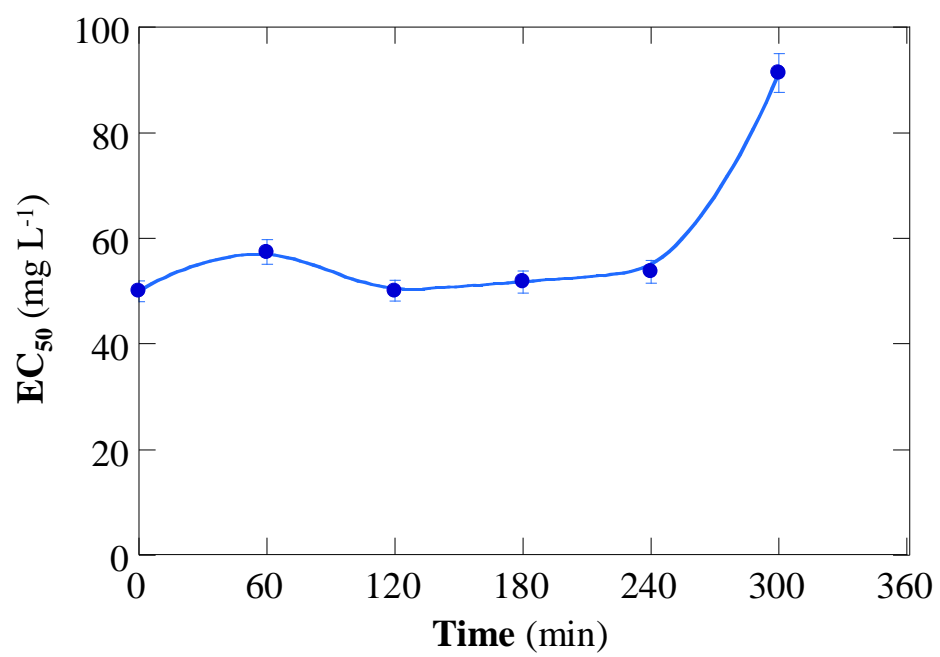
Fig. 11
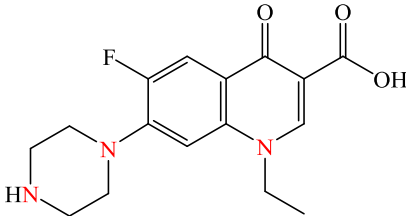
Table 1

Selected values of percentages of NFX concentration decay, TOC removal and mineralization current efficiency, as well as energy consumption per unit TOC mass, obtained with the flow system of Fig. 1 for different treatments of 3 L of NFX in several aqueous matrices under different conditions at pH 3.0, 30 ºC and LFR = 180 L h^{-1}.

Method	Anode	j (mA cm^{-2})	[Fe^{2+}] (mM)	[NFX] (mM)	k_1 (min^{-1}) (R^2)	% [NFX] decay (time in min)	% TOC removal (300 min)	% MCE (300 min)	EC$_{TOC}$ (kWh (g TOC)$^{-1}$) (300 min)
0.15 mM NaCl + 0.45 mM Na$_2$SO$_4$ synthetic solution									
AO-HClO	Ti|In–Sn–Ru	15	-	0.103	0.200 (0.994)	97 (15)	53	6.0	0.80
EF-HClO		15	0.40	0.103	0.104 (0.997)	96 (30)	49	5.2	0.83
PEF-HClO		15	0.40	0.103	0.096 (0.980)	100 (30)	39	4.0	1.03
SPEF-HClO		5	0.40	0.103	0.020 (0.980)	94 (120)	13	4.1	1.03
		10	0.40	0.103	0.071 (0.993)	100 (60)	23	4.3	0.82
		15	0.10	0.103	0.132 (0.982)	98 (30)	17	1.6	2.64
		15	0.20	0.103	0.102 (0.980)	100 (30)	39	5.0	0.84
		15	0.40	0.051	0.278 (1)	100 (10)	29	2.1	1.81
		15	0.40	0.103	0.128 (0.995)	98 (30)	46	5.7	0.75
		15	0.40	0.146	0.075 (0.996)	97 (30)	43	7.0	0.63
		15	0.50	0.103	0.078 (0.991)	100 (45)	40	5.0	0.89
		20	0.40	0.103	0.195 (0.991)	100 (15)	30	3.0	1.53
SPEF-HClO	BDD	15	0.40	0.103	0.242 (0.996)	100 (15)	60	7.5	0.73
		20	0.40	0.103	0.144 (0.997)	99 (15)	60	5.4	1.11
WWTP effluent									
SPEF-HClO	Ti|In–Sn–Ru	15	0.40	0.103	0.078 (0.985)	100 (30)	40	-	1.21

Table 2

Primary by-products detected by LC-MS/MS for the treatment of 3 L of 0.103 mM NFX in 15 mM NaCl + 45 mM Na_2SO_4 synthetic solution with 0.40 mM Fe^{2+} by SPEF-HClO, as well as in 50 mM Na_2SO_4 by AO. In both cases, trials were made at pH 3.0 and 30 ºC for 300 min, using the solar flow plant of Fig. 1 at j = 15 mA cm^{-2} and LFR = 180 L h^{-1}.

No	Chemical formula	Chemical structure	Molecular mass	Retention time (min)	Main fragmentation ions (m/z)
1	$C_{16}H_{18}FN_3O_3$		319	15.5	320, 302 (-H_2O), 276 (-CO)
2	$C_{16}H_{18}FN_3O_4$		335	14.5	336, 318 (-H_2O), 294 (-2 C), 277 (-NH_2), 251 (-C_2H_2), 233 (-H_2O)
3	$C_{14}H_{15}ClFN_3O_3$		327	16.3	328, 310 (-H_2O), 285 (-C_2H_5N), 267 (-H_2O)
4	$C_{16}H_{19}N_3O_4$		317	14.2	318, 300 (-H_2O), 274 (-CO_2), 245 (-C_2H_5), 219 (-CN)
5	$C_{16}H_{18}FN_3O_4$		335	14.5	336, 318 (-H_2O), 294 (-2 C), 277 (-NH_2), 251 (-C_2H_2), 233 (-H_2O)
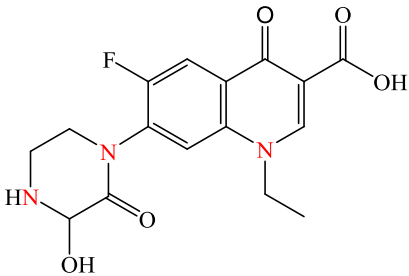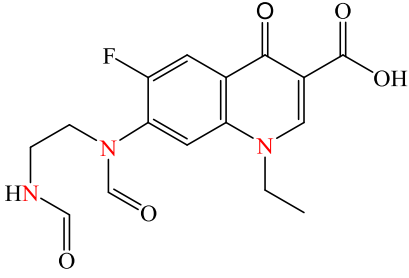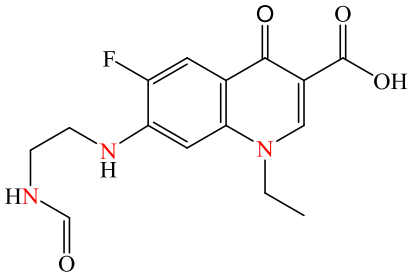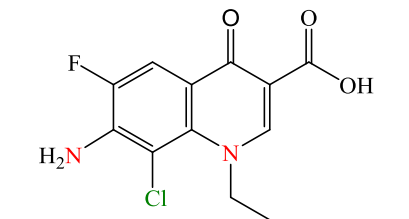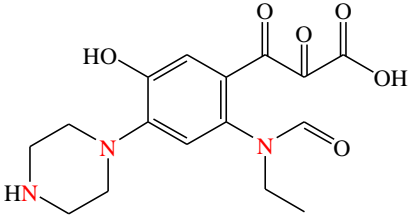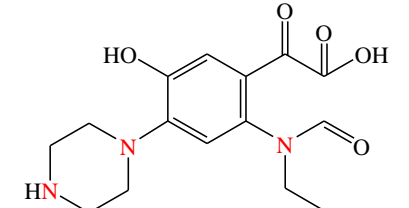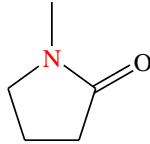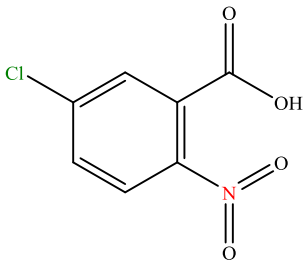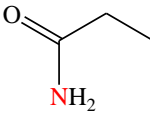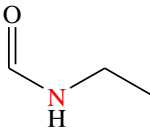
6	$C_{16}H_{16}FN_3O_5$		349	20.4	350, 332 (-H$_2$O)
7	$C_{16}H_{16}FN_3O_5$		349	20.4	350, 332 (-H$_2$O)
8	$C_{15}H_{16}FN_3O_4$		321	13.0	322, 304 (-H$_2$O), 284 (-HF), 261 (-CHNO)
9	$C_{12}H_{10}ClFN_2O_3$		284	28.0	285, 267 (-H$_2$O)
10	$C_{16}H_{19}N_3O_6$		349	20.4	350, 332 (-H$_2$O)
11	$C_{15}H_{19}N_3O_5$		321	13.0	322, 304 (-H$_2$O), 284, 261

Table 3

Stable by-products detected by GC-MS with a polar (P) or non-polar (NP) column at 15 and 120 min of the SPEF-HClO treatment of 3 L of 0.103 mM NFX in 15 mM NaCl + 45 mM Na_2SO_4 synthetic solution with 0.40 mM Fe^{2+}. The trial was made at pH 3.0 and 30 °C, using the solar flow plant of Fig. 1 at $j = 15$ mA cm^{-2} and LFR = 180 L h^{-1}.

No.	Chemical name	Chemical formula	Chemical structure	Molecular mass	Retention time (min), column
12	1-Methyl-2-pyrrolidinone	C_5H_9NO		99	20.3, P
13	5-Chloro-2-nitrobenzoic acid	$C_7H_4ClNO_4$		201 [a]	21.1, NP
14	Propanamide	C_3H_7NO		73	20.4, NP
15	N-Ethylformamide	C_3H_7NO		73	19.7, P
16	Formic acid	CH_2O_2		46	14.8, P

[a] ^{35}Cl.